Imperial College London

MEng Individual Project

Imperial College London

Department of Computing

Reconfigurable Acceleration of Transformer Neural Networks with Meta-Programming Strategies for Particle Physics Experiments

Author:
Filip Wojcicki

Supervisor:
Prof. Wayne Luk

Second Marker:
Prof. Alexander Tapper

June 16, 2022

Abstract

Particle Physics studies the fundamental forces and elementary particles building the Universe. In order to verify the correctness of the theories, countless experiments have to be designed and carefully executed, with the main driving force of the myriads of engineers, physicists and researchers at the Large Hadron Collider (LHC) operated by the European Organization for Nuclear Research (CERN). With the unprecedented experiments' scale comes the challenge of accurate, ultra-low latency decision-making. Transformer Neural Networks (TNN) have been proven to accomplish cutting-edge accuracy in various domains, including classification for jet tagging, which is the target of this project. However, software-centered solution implemented for CPUs and GPUs lack the inference speed needed for real-time particle triggers.

This report proposes two novel TNN-based architectures efficiently mapped to Field-Programmable Gate Arrays (FPGAs). The first one outperforms the current state-of-the-art models' GPU inference capabilities by roughly 1000 times while maintaining comparable classification accuracy. The second one trades off some of its speed for accuracy and undergoes a broad design-space exploration, which involves both pre-training and post-training quantization. The latter one leverages a custom-developed tool chain that augments existing solutions in terms of granularity and ease-of-use while following an innovative algorithm for relatively quick convergence.

Confirm this number

In this project, several recently researched neural network components are designed to target FPGAs using High-Level Synthesis (HLS). The resulting open-sourced building blocks are both highly customizable and abstract, and aim to bridge the gap between hardware and software development, effectively reducing the time and complexity needed for creating efficient neural network hardware accelerators.

Acknowledgements

I would like to express my gratitude to Professor Wayne Luk for his guidance, insightful suggestions and constant encouragement throughout the project.

I would like to thank Professor Tapper for giving me a different view on the project's meaning and providing with the behind-the-scenes information about the LHC.

I want to thank Zhiqiang Que for his continuous technical support, our weekly meetings and always being available to answer any of my questions.

Lastly, I am very grateful for my family whose support was invaluable during this project and the degree as a whole.

Contents

List of Figures

List of Tables

List of Listings

List of Algorithms

Chapter 1

Introduction

1.1 Motivation

LHC is the world's highest-energy particle collider that is capable of producing and detecting the heaviest types of particles that emerge from events such as proton-proton collisions. The detection is a challenging process as some particles, like quarks and gluons, cannot exist on their own, and they nearly instantly combine which results in collimated sprays of composite particles (hadrons) that are referred to as jets [1]. The initial particles created upon collision and their behaviors are of main interest of the physicists, which leads to jet tagging - the challenge of associating particle jets with their origin.

There are many detector types used for the analysis of the particle collisions, each based on a different physical phenomenon, which results in availability of both higher and lower level features from each event. The former have been successfully used in the past using more physically motivated machine learning (ML) algorithms, e.g. using computer vision [2]. However, more recently, various deep learning approaches have proven to outperform their predecessors [3]. It has also been found that all the detected features carry the same underlying information, with convolutional neural networks trained on higher-level data achieving nearly identical accuracy as dense neural networks trained on the data from the other end of the spectrum [4].

The information throughput of Petabytes per second collected by the LHC detectors outclasses the real-time inference capabilities of the typical state-of-the-art solutions. The real-time decision-making is often of utmost interest, hence this paper is motivated by this challenge which includes exploring various types of neural network architecture as well as the necessary infrastructure and deployment processes. Recently, ***hls4ml*** codesign workflow have been successfully adopted in particle physics experiments [5], which allows ML researchers and physicists to easily deploy their solutions trained using common ML frameworks on reconfigurable or application specific hardware, vastly improving the detection algorithms' inference capabilities. However, *hls4ml* lacks support for a number of neural network architectures that have been proven to outperform the previous state-of-the-art, including graph neural networks [6, 7] and transformer neural networks [8].

1.2 Objectives and Challenges

The purpose of this project is to develop novel, hardware-aware neural network architectures as well as to establish efficient ways mapping them onto FPGAs. Another objective is to use metaprogramming strategies to integrate them into the *hls4ml* library or standalone tools, with various optimizations approaches that offer trade-offs between latency, throughput and hardware resources usage. Hence, there is an emphasis on creating parametrizable and reusable designs that can support creation of ultra-low latency systems, effectively transforming proof-of-concept implementations into optimized hardware accelerators.

The two main challenges of the project involve:

- **C1**: Developing deep and complex neural network models with inference times in the microseconds range, which requires much lower abstraction levels than a typical ML framework. It is also crucial to stay aware of the underlying hardware architecture to exploit its strengths while keeping compile-time and run-time configuration easily accessible.
- **C2**: Bridging the abstraction gap for the translation between high-level representation of neural networks and their optimized mapping to hardware. The design space exploration is a long and difficult process, which needs careful examination and analytical performance models to find the optimal solutions.

1.3 Contributions and Publication

The project aims to benefit the open-source community of ML practitioners and researches that are in need of faster and more parametrizable neural network inference. The main audience for that operation are particle physicists, nonetheless, the hope is for the work to positively contribute many ML fields by offering a reliable tool for acceleration of existing designs and providing a useful resource for learning about the nature of reconfigurable hardware and its optimization potential.

The novel aspects proposed in this work can be summarized as follows, with the first two addressing challenge **C1**, and the latter challenge **C2**:

- **Hardware-Aware Network Optimizations**: Two novel architectures are designed with hardware in mind, exploiting the target hardware platform to achieve cutting-edge latency and accuracy.
- **Efficient Hardware Implementation**: `hls4ml` codesign workflow is extended with a number of complex neural network layers that benefit from a range of optimization techniques.
- **Quantization-Aware Transformer Neural Training**: Several available solutions are surveyed and described, and the best one in terms of applicability to state-of-the-art neural network designs is selected and adapted to Transformer Neural Networks.
- **Custom Post-Training Quantization**: A custom tool is proposed that finds the optimal set of bit-widths for a High-Level Synthesis model according to used-defined constraints.

The bulk of the work and analysis conducted in this project was summarized in the paper "Accelerating Transformer Neural Networks on FPGAs for High Energy Physics Experiments" and submitted in the long paper category to the *18th International Symposium on Applied Reconfigurable Computing*. A journal article derived from this project is being prepared for publication.

1.4 Report Outline

This report begins by discussing the necessary particle physics background to understand the scope of the work, followed by the related work in the field of machine learning, with an emphasis on the state-of-the-art architectures, and a deeper dive into the reconfigurable hardware technology in chapter 2. Then in chapter 3, the two proposed novel neural network architectures are described in details, including the necessary training and processing steps. After that, chapter 4 covers both the existing and custom ways of conducting design space exploration and how they were applies in this project. Chapter 5 discusses the evaluation metrics and collected experimental results, which is concluded by chapter 6, which also proposes future work derived from this analysis.

Confirm at the end if the sections are still as described here

Chapter 2

Background and related work

This chapter provides a closer look at the concepts required to understand this work. The following sections firstly discuss background and related work for topics in particle physics, then machine learning and finally reconfigurable hardware research. At the end of this chapter, the ethical issues that could arise from the project are listed and discussed.

2.1 Particle Physics

To be able to understand the scope of the project and the applicability of the work in modern research, this chapter gives an overview of the key concepts from particle physics that appear through the paper. The explanation is written for readers with no prior background in physics.

2.1.1 Standard Model

the Standard Model is a theory that describes the connections between weak, strong and electromagnetic interactions, which are three of the fundamental forces. The possible unification with the forth one - gravity - is an ongoing research [9], and while certainly outside the scope of this project, it should be noted that some of the physical experiments that this work explores aim to help with it [10, 11].

The Standard Model also provides a classification of all the elementary particles. A non-exhaustive list of them is described below, with particles that this report is concerned about (as they appear in the proton-proton collisions) being highlighted.

- Fermions
  - Leptons - participate in electroweak interactions; include electron (e^-)
  - Quarks - participate in strong interactions; include **light quarks (q)**[1] and **top (t) quark**
- Bosons
  - Gauge bosons - force carriers; include photon (γ), **W boson (W^+, W^-)**, **Z boson**, **gluons**
  - Scalar bosons - give rise to mass; include **Higgs boson (H^0)**

The information about the following decay processes form the dataset of this report, with visualization in figure 2.1 (obtained from [6]). It is important to note that where applicable, the particles on the left-hand side of the arrows undergo a series of decays before reaching the right-hand side, when the only particles left are those composed of quarks and antiquarks (denoted by the vertical bar), referred to as hadrons.

Possibly clear page

$$q/g$$

$$H^0/W/Z \rightarrow q\bar{q}$$

$$t \rightarrow Wq \rightarrow q\bar{q}q$$

[1] Light flavor quarks: up (u), down (d), charm (c), and strange (s) quarks

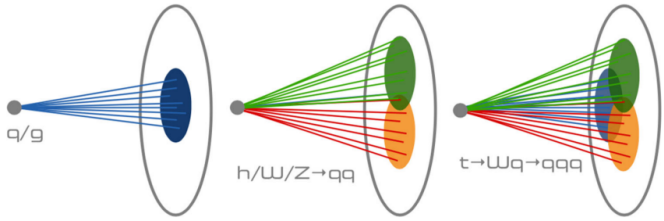

Figure 2.1: Representation of different decay processes, based on the number of resulting jet clusters.

2.1.2 Particle Accelerators and Triggers at LHC

The two LHC experiments that are of most concern in this report are CMS and ATLAS. They are both large general-purpose particle detectors, that were notably involved in the discovery of the Higgs boson [12]. Several processing steps happen between particles colliding and theories being proven, however real-time particle detectors comprises the very first elements of this pipeline. They are composed of triggers split into the following levels [13, p.16]:

- **Level 1 trigger (L1T)** - it is implemented in hardware (FPGAs) and firmware, it is pipelined (a term explained in details in subsection 2.3.5) and it cannot allow for any dead-time, which means that it has to continuously process data with a fixed latency.
- **Level 2 trigger (L2T)** - it is implemented in hardware and software and can include regional processing.
- **Level 3 trigger (L3T)** - it is implemented in software, using farms of CPUs. It is close in behavior to non-real-time algorithms.

LHC operates in intertwined periods of operation and shutdown. The latter come from the demanding nature of the experiments that necessitates maintenance and upgrades to the apparatus and machinery, as well as the science and engineering advancements which allow for more efficient algorithms and technologies to be adopted. Very recently, after four years of break, LHC restarted experiments, which marks the beginning of "Run 3" [14]. Since their origin, the L2T and L3T have been merged into High Level Trigger (HLT) [15, p.47], which is planned to rely on thousands of multithreaded CPUs and GPUs. As for the L1T key specifications that will be used to evaluate the design in this paper, its input data frequency is 40 MHz, which with a pipeline depth of 500 results in a 12.5 μs latency, and its output frequency to HLT is equal to 750 kHz.

2.1.3 Dataset and Notations

The datasets used in this work has been simulated to mimic the 13 TeV proton-proton collisions performed at LHC, and it includes information about the most energetic jets [16] (30 [17], 50 [18], 100 [19] and 150 [20]) that were constructed using the anti-K_t clustering algorithm [21]. A number of jet representations are available in the dataset:

- High level features (HLF), which are physically inspired,
- Images, which are related to an energy heat-map,
- Constituent list, which contains jets' constituent hadrons from the following list: light quarks, top quarks, W bosons, Z bosons, and gluons.

Compared to the other two, the constituent list is a lower-level representation, however, as mentioned in chapter 1, this should not affect the classification accuracy [4]. It is also worth mentioning that a simpler dataset that contains only the HLF jet representation [22] is also used in this project as it vastly reduces the complexity of a design while offering comparable accuracy. A more thorough discussion between the differences in their use cases is carried in chapter 5, but it is worth mentioning that the HLF representation has been successfully used in conjunction with deep neural networks [23], while the images and constituent lists were adopted for graph neural networks [6].

To facilitate further analysis, this subsection also explains the notation used for the dataset as it is important throughout the report. Each constituent element $\boldsymbol{x^l}$ is a 16-dimensional vector, where l denotes the index in the list:

$$\boldsymbol{x^l} = \begin{bmatrix} x_0^l & x_1^l & \dots & x_{15}^l \end{bmatrix}^T \in \mathbb{R}^{16} \tag{2.1}$$

The physical meaning of each element's dimension is not taken into consideration, and all of them are treated as equally important. A constituent list $\boldsymbol{x^i}$ acts a single sample, with index i within a dataset, and it varies in terms of the number of constituents L, but it has no more of them than the dataset name suggests:

$$\hat{\boldsymbol{x^i}} = \begin{bmatrix} \boldsymbol{x^{i,0}} & \boldsymbol{x^{i,1}} & \dots & \boldsymbol{x^{i,L-1}} \end{bmatrix} \in \mathbb{R}^{L \times 16} \tag{2.2}$$

Using the 30 jet dataset as an example, each sample has between 1 and 30 constituents, although in the majority of samples it is the upper boundary. Hence, the whole dataset with N samples can be represented as D:

$$D = \begin{bmatrix} \hat{\boldsymbol{x^0}} \\ \hat{\boldsymbol{x^1}} \\ \vdots \\ \hat{\boldsymbol{x^{N-1}}} \end{bmatrix} = \begin{bmatrix} \boldsymbol{x^{0,0}} & \boldsymbol{x^{0,1}} & \dots & \boldsymbol{x^{0,L-1}} \\ \boldsymbol{x^{1,0}} & \boldsymbol{x^{1,1}} & \dots & \boldsymbol{x^{1,L-1}} \\ \vdots & \vdots & \ddots & \vdots \\ \boldsymbol{x^{N-1,0}} & \boldsymbol{x^{N-1,1}} & \dots & \boldsymbol{x^{N-1,L-1}} \end{bmatrix} \in \mathbb{R}^{N \times L \times 16} \tag{2.3}$$

The main jet datasets contain $880,000$ samples regardless of the number of jets per sample, while the HLF dataset contains $830,000$ examples, which are split into training and test samples in $70:30$ and $80:20$ proportions accordingly. In both cases, the datasets are balanced, meaning that they contain all available particle classes in near identical proportions. This is a desired characteristic of data as it avoids having to introduce weighted results as a measure of protecting the model from not learning the underrepresented classes properly. When it comes to the distribution and range of values for each feature, the visualizations can be seen in figure 2.2

Maybe city the OpenML website

and TODO for HLF and constituent list datasets respectively.

It is also worth mentioning that normalization[2] is the only preprocessing measure used in this work, and it is only applied to the HLF dataset. The reasons behind avoiding it in case of the constituent list dataset are discussed in detail in section 3.3. Both dataset samples are simulated and do not contain any illegal or null values that would require dropping or substituting. There is also no need for data augmentation because of the simulated origin of data.

Constituent list feature distribution

[2]Process of subtracting mean and dividing by standard deviation, also referred to as "standardization".

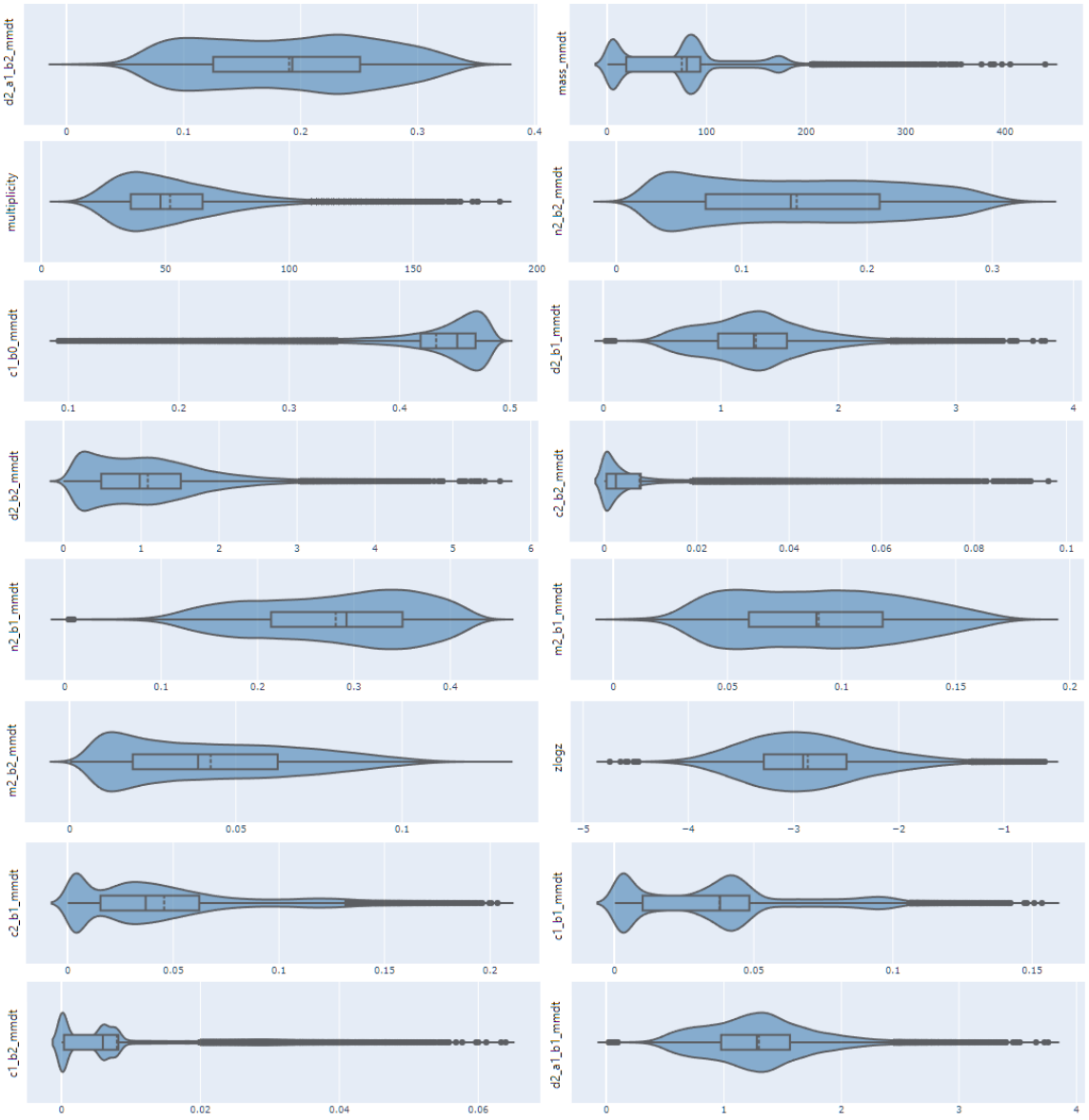

Figure 2.2: Representation of the distributions of feature values in the HLF dataset.

2.2 Machine Learning

Neural networks belong to a wider field of machine learning (ML) - the study of using experience to improve algorithms. This section assumes a basic understanding of ML and gives a brief overview of the topics needed to understand the scope of the project. It then explains in more details the background and related work for the architectures involved in this research.

2.2.1 Metrics

There are several key metrics used for assessing the success of an ML algorithm, and the following will be used throughout the report:

- **Classification accuracy** - a simple measure of the percentage of correctly classified samples.
- **Area Under the Curve (AUC) for the Receiver Operator Characteristic (ROC)** - a more complex measure of the model's ability to correctly distinguish between classes. It can be used similarly to the classification accuracy, but it favors discriminative over representative models.
- **Confusion matrix** - a tabular metric that compares the actual samples' classes with the predicted ones, effectively categorizing results into four groups: true positive, false positive, false negative, and true negative. This allows for an easy calculation of precision and recall values.

Give equations for TPR, FPR, AUC etc.

Explain when accuracy is not enough and AUC and confusion matrix gives a better picture

2.2.2 Deep Neural Networks

While there exist a number of ML techniques that have proven successful for various use cases at LHC, like Support Vector Machines [24] or Boosted Decision Trees [25], in the last years deep neural networks (DNN) have been proposed with improved results for applications like infrastructure monitoring [26], offline data analysis [27], and the main interest of this report - detectors' trigger mechanisms.

In many uses cases the neural networks architectures are optimized and accelerated to shorten the training time (measured in hours or even days) to reduce the time needed for evaluating different design configurations and easily performing the hyperparameter search. However, this work focuses on accelerating the inference to match the extremely low latency required in the LHC detectors' L1 triggers. Although often measured in milliseconds, sub-milliseconds inference time has been achieved for this application with the use of FPGAs using architectures for basic DNN [22], and recently sub-microseconds latency for graph neural networks (GNN) [28, 29]. These implementations serve as a baseline latency for this project which aims to achieve comparable performance with higher AUC value.

Figure 2.3 shows an overview of a fully connected neural network with one hidden layer, which allows to derive the mathematical formulae. Each layer consists of neurons which hold a value, which means that input, output and the intermediate hidden layer can be modelled similarly. The arrows between neurons represent learnable weights, while the (optional) biases involved in the calculation, denoted as b, can be depicted as arrows from the "bias neurons", in all but the last layer. The value of a neuron depends on all the neurons in the previous layer as well as the weights and biases between them, which can be formulated into the equation 2.4 using the hidden layer as an example:

$$h_0 = f(w_{i,0} \cdot i_0 + w_{i,1} \cdot i_1 + \ldots + w_{N-1} \cdot i_{i,N-1} + b_{i,0}) = f(\sum_{j=0}^{N-1} w_{i,j} \cdot i_j + b_{i,0}) \tag{2.4}$$

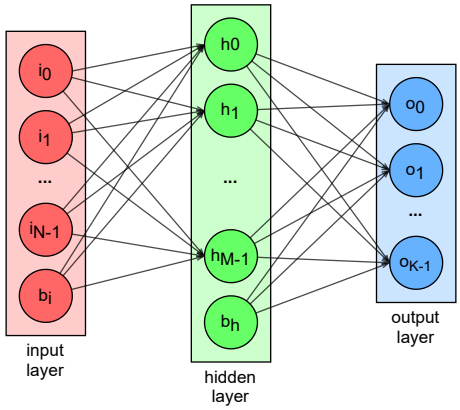

Figure 2.3: Diagram of a fully connected layer.

What is also not displayed in the diagram, but can be seen in the equation is the activation function f that is required to introduce non-linearity in the computations. Without it, all consecutive layers involving solely multiplication and addition could be simplified to s a single layer thanks to the distributive property in linear algebra, defeating the point of having multiples of learnable parameters. The activation function can be as simple a piece wise linear function called Rectified Linear Unit (ReLU) defined in equation 2.5:

$$\text{ReLU}(x) = \max(x, 0) = \begin{cases} x & \text{x} > 0 \\ 0 & \text{otherwise} \end{cases} \tag{2.5}$$

or more complicated like the Sigmoid Linear Unit (SiLU), based on the sigmoid function, both presented in equation 2.6

$$\text{SiLU(x)} = x \cdot \sigma(x) = x \cdot \frac{1}{1 + e^{-x}} \tag{2.6}$$

As layers are tightly connected to each other, this type of neural layer is often referred to as *fully connected* or *linear*. It requires a relatively large number of separate weights and biases, which makes it both computationally and memory intensive, but nonetheless, modern network architectures can have dozens of these layers, not to mention plethora of other types.

2.2.3 Convolutional Neural Networks

Quick introduction and visualization of CNNs as other notable jet-tagging algorithms use them and are mentioned in this report

2.2.4 Graph and Recurrent Neural Networks

Quick introduction and visualization of graph and recurrent (including GRU and LSTM) NNs as other notable jet-tagging algorithms use them and are mentioned in this report

2.2.5 Batch and Layer Normalization

Batch norm vs layer norm as both are used in the architecture

2.2.6 Transformer Neural Networks and Self-Attention

A promising architecture that has been chosen as the topic of this project is the transformer neural network (TNN). Similarly to RNNs, TNNs were designed for sequential input data, most commonly found in natural language processing applications, however, compared to RNNs, they process all input data at once. In RNNs, convolutional [30] or attention mechanisms [31] are used in a recurrent manner to allow models to learn the representation and connections between different parts of the input sequence, which most commonly are words in a sentence. This limits the parallelizability as the network is handled serially - each hidden state needs to wait for the result generated by the previous one. In TNNs, a modified mechanism called self-attention [32] is used which can find global relations in a data, without relying on the temporal, sequencing information. The self-attention combines several simpler operations to achieve its strength, including linear layers, matrix multiplication and the softmax function, formula for which is presented in equation 4.4.

$$\text{softmax}(x) = \frac{exp(x_i)}{\sum exp(x_i)} \tag{2.7}$$

Softmax can be described as mapping a vector to a ratio between each input's exponentiation result and the sum of all such values, which gives the property of the resulting vector entries sum equal to one. This characteristic means that the output can be treated as vector of probabilities, which is often exploited in the final activation layer of a neural network.

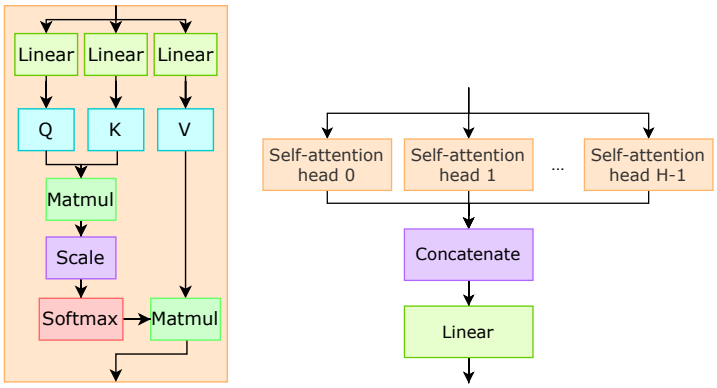

Figure 2.4: Left: diagram of a self-attention head. Right: illustration of H self-attention heads forming a multi-headed self-attention block.

A diagram representing the initial implementation of the self-attention can be seen on the left in figure 2.4. The Q, K, and V stand for *queries*, *keys*, and *values* respectively, which although arbitrary, are meant to give a better understanding behind the idea of this mechanism. It is also important to note, that multiple blocks of self-attention, referred to as *heads*, can be used together, which allows for each head attending information about a different hidden characteristic of an input. The results of all heads are simply concatenated, increasing output's dimensionality, and multiplied with a learned weight, as seen on the right in figure 2.4. To better comprehend the interactions between information learned by the heads, figure 2.5 shows a visualization for 1, 2 and 8 heads on an example sentence, obtained using Tensor2Tensor library [33, 34]. While it is quite clear in the example that "it" is mostly associated with "The" and "animal" with 1 attention head, the interpretability is worse in case of 2 and 8 attention heads.

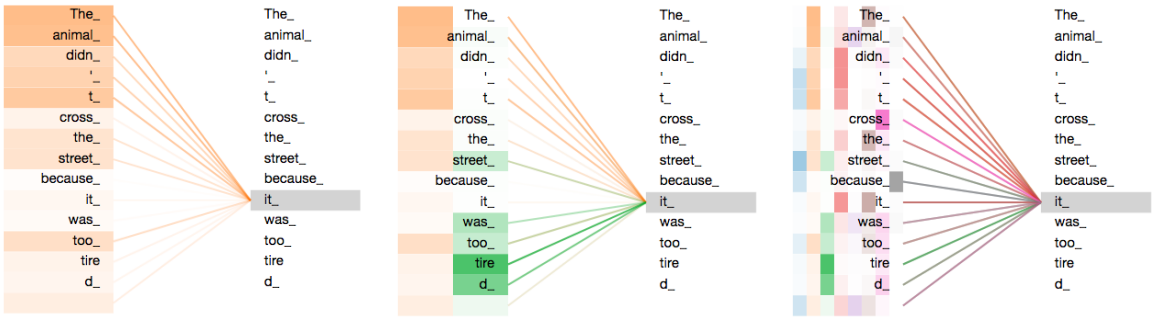

Figure 2.5: From left to right: visualizations, for an input word, of the words focused by 1, 2 and 8 attention heads.

The complexity of a multi-head self-attention depends on the dimensions of the underlying *queries* $\in \mathbb{R}^{N_Q \times d_Q}$, *keys* $\in \mathbb{R}^{N_K \times d_Q}$, and *values* $\in \mathbb{R}^{N_K \times d_V}$ parameters. The resulting time complexity is represented in the equation 2.8, while the space complexity can be seen in equation 2.9 with h and d_{out} standing for number of heads and output dimensions respectively in both cases.

Cite or derive this complexities

$$\mathcal{O}(h \cdot (N_Q N_K (d_Q + d_V) + d_Q^2 (N_Q + N_K) + d_V^2 N_K + N_Q d_V d_{out}))) \tag{2.8}$$

$$\mathcal{O}(h \cdot (N_Q (N_K + d_V) + d_Q (N_Q + N_K) + d_V N_K + N_Q d_{out}))) \tag{2.9}$$

It has to be mentioned that in terms of the AUC value, a recent implementation of a transformer called ConstituentNet [8] has been shown to outperform previous state-of-the-art GNN implementations like JEDI-net [6] and thus serves as an inspiration for the starting point architecture of chapter 3, which is entirely devoted to a further analysis of the network design and suitability for

jet tagging. More specifically, given the strong results of its software implementation, an FPGA-mapped design is believed to have a possibility to be a viable alternative to existing designs for L1T at LHC.

2.3 Reconfigurable Hardware

A significant portion of the project's work involves exploiting reconfigurable hardware to vastly reduce the inference time of the proposed neural networks. This section explains in more detail the technology and characteristics of reconfigurable hardware, and in particular, FPGAs.

2.3.1 Landscape of Hardware for Computing

The modern landscape of digital integrated circuits (IC) is very rich can be divided into numerous categories depending on the technology used and expected functionality [35]. A list of platform types is described below, with the emphasis of their suitability for neural networks applications.

- **Central Processing Units (CPU)** - the most commonly found ICs that are at the core of personal computers, laptops and handheld devices. They are capable of executing a broad range of predefined instructions. As CPUs have become widely adopted in research long before the emergence of the other technologies from this list, they were the first platforms for the training and inference of neural networks with promising results back in the 1980s and 1990s for applications like high energy physics [36] or biology [37]. Although it is possible to achieve speed-ups of over 10x the baseline performance with careful optimizations [38], CPUs are now consistently outperformed by more suitable technologies, and only limited to certain inference tasks.
- **Graphic Processors (GPU)** - ICs originally specialized in graphics processing intended for displaying images. Since their inception, due to the type of calculations involving matrix and vector operations, other applications related to cryptography and neural networks have also adopted GPUs as their main platform. In the former domain, cryptocurrency mining has transitioned from CPU to GPU to increase profitability [39], while for the latter, the more powerful hardware drastically reduced training and inference times, thus allowing for deeper and more complex architectures yielding higher accuracy [40, 41].
- **Application Specific Integrated Circuits (ASIC)** - as suggested by the name, those are the custom designed ICs heavily specialized for a particular application. It is hard to generalize them, as the use cases can cover any modern computing problem, but the commonality is a vast improvement in performance and power usage compared to more general purpose solutions. However, the long and expensive development process pose extremely high barriers to entry for most users. Fortunately, off-the-shelf products like the Graphcore Intelligence Processing Units [42], that are designed specifically with machine learning applications in mind, as well as other custom designs [43, 44] are starting to offer a compelling platform for working with neural networks.
- **Field-Programmable Gate Arrays (FPGA)** - differently from the previous listed IC types, FPGAs are not manufactured for a specific use case, and in fact, they can be reprogrammed to be a platform for a different application at any time. The reprogrammability comes at a cost of performance and power consumption compared to ASICs [45], but at the same time outperforms GPUs in these regards [46, 47]. It is also suggested, that with some technological improvements focused on ML applications, FPGAs can narrow the gap between ASICs without needing to stick to one particular design [45, 48, 49].

FPGAs offer an interesting trade-off between implementation effort and acceleration potential when it comes to neural networks and for that reason they have been chosen as the target technology in this report. The following subsections give a closer look at some of their characteristics and associated tools.

FPGA lattice overview to visualize explain the idea behind this technology

|

|

|

2.3.2 High-Level Synthesis

For many years, FPGAs have been modelled using register-transfer level (RTL) design abstraction with the use of hardware description languages like Verilog or VHDL. However, to increase productivity and allow for a more convenient design state space exploration (DSE), a more abstract modelling process called High-Level Synthesis (HLS) can be adopted. The design can be expressed in a software programming language like C, C++ or Java, which can be both manually and automatically optimized, and transformed to an equivalent RTL. This is especially beneficial in research, where compared to industrial environment, it is more likely that a slightly lower quality of results can be afforded for increased productivity and easier DSE. In fact, a recent study shows that on average only one third of design time and half of the lines of code are needed for an equivalent project done in HLS in comparison to RTL while the quality of results varies and can even outperform the RTL implementations for some applications [50].

This report's work is based on Xilinx Vivado HLS design suite. When developing a solution, it is important to note, that the synthesis process can take a significant amount of time (from a couple of hours to days on a modern powerful machine), and so there exist two simulation methods - a C-simulation that can quickly and directly evaluate a software benchmark against an emulation of the design, and a more truthful, cosimulation that firstly synthesizes a design and accompanying test bench to RTL and then performs an RTL simulation. A final, definitive evaluation of the results requires programming a target FPGA with the generated bit stream of the design and exchanging input/output data with a program that usually runs on a CPU.

HLS to RTL flow diagram

|

|

|

2.3.3 `hls4ml` Codesign Workflow

A commonality between the recent best performing hardware-mapped neural network models is the use of the *hls4ml* codesign workflow that was mentioned in section 1.1.

More about hls4ml

Difficulty: rtl > hls > python hl4ml, draw comparison with assembly

|

|

|

|

|

|

|

|

2.3.4 Latency, Throughput, and Hardware Resources

To properly navigate during the DSE and assign scores the solutions, the following characteristics have to be considered:

- **Latency** - A time measure of a system between receiving an input signal and producing a *corresponding* output. It is crucial in real-time processing where it has to be lower than the period between subsequent input samples. Depending on the application, latency in the microseconds or nanoseconds range can be expected from an FPGA. To recall from section 2.1.2, the latency constraint for this work comes from the specification of L1T at LHC and is equal to 12.5 μs.
- **Throughput** - A rate of samples processed in a unit of time. For architectures that only start to process new elements after the previous one has finished, it is directly linked to latency. However, in modern ICs, especially in FPGAs, it is one of the defining metrics of performance and designs tend to exploit pipelining and parallelizability to marginally trade off their latency to increase it. Despite that, in this work, this measure is of little interest given the fixed latency and no dead-time constraint of L1T.
- **Resource utilization** - A more complicated, often multidimensional, metric that describes either the raw number or ratio of total usage of the hardware components of an FPGA. Typically, the higher it becomes, the more power is drawn by an FPGA, however, it is most often used to guide the design process to avoid running out of a certain resource. This can be done by potentially deploying an alternative method that can be implemented using a different, less contested resource.

While FPGAs vary in terms of hardware resource configurations, several key components can be distinguished:

- **Block Random Access Memory (BRAM)** -

  finish

- **Digital Signal Processing (DSP) logic element** -

  finish

- **Flip-Flop (FF)** -

  finish

- **Lookup Table (LUT)** -

  finish

To fully understand the trade-offs between designs, one cannot forget about the metric directly related to the specific task that is accelerated in hardware. In the case of this report, classification accuracy and AUC described in section 2.2.1, will also play key roles in evaluating various configurations.

2.3.5 Serial, Parallel, and Pipelined Architectures

Hardware architectures use components that can be configured in different ways depending on the overall goal or a limiting factor. The high-level configurations of building blocks are displayed in figure 2.6 and can be described as follows:

- **Serial** - elements are arranged in a chain, processing one after another. This way uses less resources than an equivalent parallel configuration by reusing given components R times, thus approximately trading-off R times less required resources for R times higher latency.

- **Parallel** - elements share a common input and start processing data at the same time. This way ends in a lower latency than an equivalent serial configuration consuming using more resources.

- **Pipelined** - a more sophisticated arrangement, in which subsequent processing blocks (that can be either placed serially or in parallel) form a pipeline of processing stations separated by simple storage elements called pipeline registers, implemented using FFS. This maximizes the usage of the design blocks, hence increasing throughput with a minimal sacrifice of latency and resource usage.

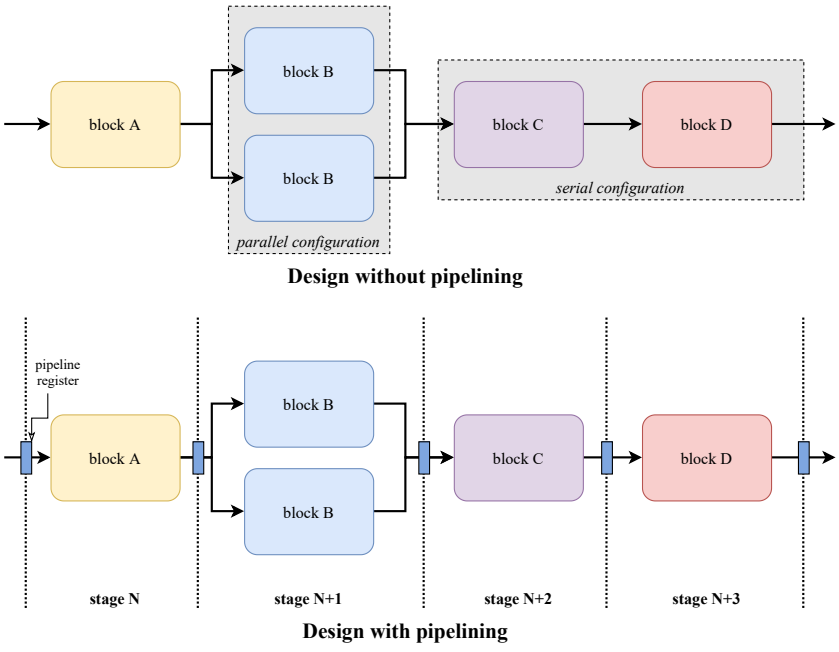

Figure 2.6: Diagram comparing serial and parallel configurations as well as showcasing designs with and without pipelining.

2.3.6 Pareto Front and Roofline Model

To make an informed design decision, various architectures can be compared by arranging them on a dependency graph (e.g. latency vs resource usage) and observing the Pareto front - the set of solutions for which there are no better ones in regard to one quality given that the other measure is not worse. The slightly complex definition can be easily understood from figure 2.7, which also highlights another use of this method - finding design configurations that are yet to be explored.

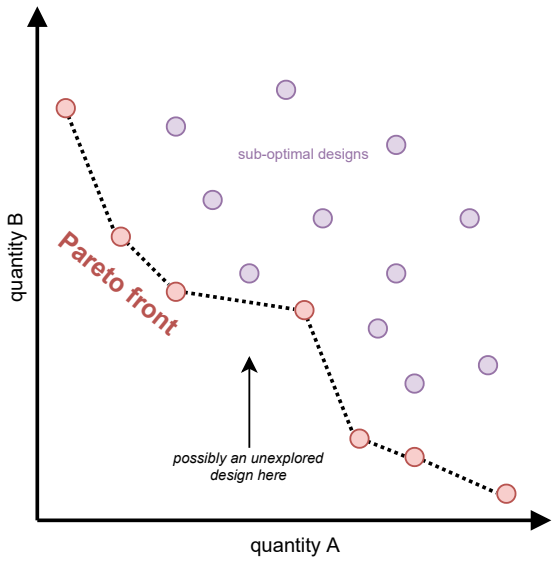

Figure 2.7: Example graph with designs plotted against quantities A/B, Pareto front highlighted.

Another intuitive performance visualization comes in the form of the Roofline model, which compares the obtained results with theoretical limits coming from inherent hardware limitations like clock frequency or memory bandwidth. An example can be seen in fig 2.8.

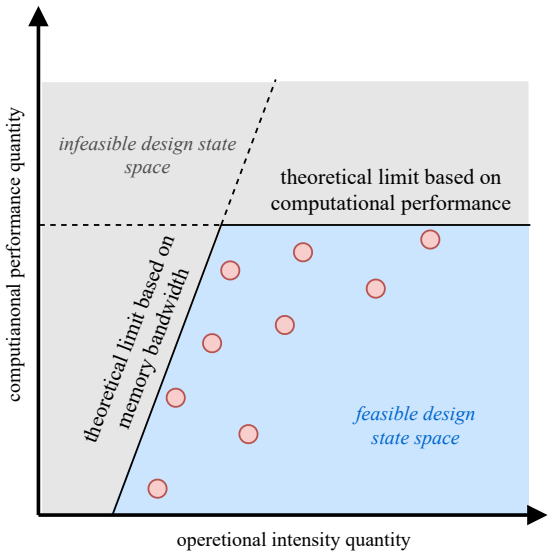

Figure 2.8: Example graph with computational and memory bandwidth limitations showcasing the Roofline model

2.4 Ethical Considerations

The purpose of this project is to advance the next-generation particle physics experiments. There are two main aspects that need to be considered - the development of a hardware-mapped transformer neural network architecture and the easy-to-access translation and optimization toolchain for efficiently expressing and networks in common machine learning frameworks.

The first feature is aimed at a purely civilian, scientific audience, and it is tailored towards particle collision datasets. With that in mind, it is important to mention that, as with most machine learning research, there is potential for a misuse of the acceleration techniques towards a military or malevolent application that could negatively impact the society. However, this also means that there is a low risk for new emerging threats from this particular work; rather the already present ones could become slightly more serious. Fortunately, this should result in existing harm prevention measures staying intact or solely requiring adjustments to their accuracy or speed thresholds.

With the second element's goal of making the creation and deployment of neural networks more accessible, it could be argued that this may in turn increase the number of high energy physics experiments requiring immense energy consumption, like those at LHC [51], thus negatively affecting the environment. However, this is considered a very low likely cause of action, as the research work of this project is aimed at helping already running experiments and more importantly, the negative environmental implications (for which there are various mitigation strategies [52, 53]) are heavily outweighed by potential beneficial technological advancements coming from the scientific discoveries.

Aside from the aforementioned ethical issues, the project is aimed at benefitting the open-source scientific community world-wide. Its outcome could lead to a much more accessible and efficient inference methods that are applicable in many domains outside particle physics.

Chapter 3

Architecture Exploration

This chapter presents the proposed neural network architectures. It starts with a baseline TNN network implemented in `PyTorch`, which then undergoes a series of hardware-aware adaptions specific to jet tagging. During this process two separate architectures are developed, which differ by the input type and design goal. The first one, referred to as the *ultra-low latency* one, targets the HLF jet representation and aims to achieve the lowest possible latency at the cost of accuracy and AUC values. The second one, called *accuracy-focused*, is based on the constituent list jet representation and trade-offs latency for quality of classification while still remaining within L1T timing constraints. In the end, the mechanism of quantization-aware training is explained, with a proposed way of implementing it in this project.

3.1 Base Architecture

The starting point of this analysis is derived from transformer architecture used in the original paper [32] and recent proof-of-concept used for jet tagging [8]. The overview of the network components can be seen in figure 3.1.

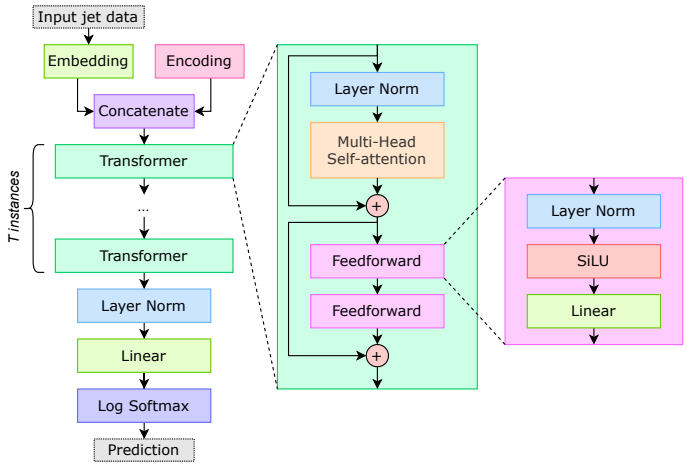

Figure 3.1: Diagram with an overview of the baseline architecture.

The straight-forward path between model's input and output highlights the sequential nature of transformer which stands in opposition to recurrency present in GRU and LSTM models. While this allows for the aforementioned parallelizability and pipelining on FPGAs, it also poses a challenge of increased hardware footprint and synthesis complexity when compared to recurrent models, where the key components can get reused to meet the resource constraints. To better understand the transformer's complexity, the next subsections derive the equations linking the internal components and explain the involved terminology.

3.1.1 Input embedding and Residual Connections

Although the model lacks any recurrency, the transformer includes two residual connections which have been widely adopted since their successful application in ResNet neural networks [54]. They offer improvements to training time and resulting accuracy [55], however, they require standardized data dimensionality to ensure the summation can be logically executed. In this project, this is obtained thanks to input embedding, which transforms the input $\hat{\boldsymbol{x}}^{\boldsymbol{i}} \in \mathbb{R}^{L\times 16}$ into a shape $\mathbb{R}^{L\times d}$ that is used through the design, as seen in equation 3.1. The d size is referred to as the self-attention latent or embedded dimension.

$$\hat{\boldsymbol{x}}^{\boldsymbol{i}}{}_{\text{emb}} = \text{embedding}(\hat{\boldsymbol{x}}^{\boldsymbol{i}}) = w_{\text{embed}}\ \hat{\boldsymbol{x}}^{\boldsymbol{i}} + b_{\text{embed}} \in \mathbb{R}^{L\times d} \tag{3.1}$$

This dimensionality change can be conveniently performed using a linear layer, and it has to be remembered that each such layer increased the model learning capacity thanks to the learnable weights and bias. The network's inner dimension d is treated as a hyperparameter as it influences the model's accuracy and performance, but it has to be noted that the other dimension prevalent in the network comes from the input's number of jet constituents L (which is set to 1 in case of the HLS representation), meaning that the model is also susceptible to a parameter which cannot be easily tuned.

3.1.2 Input Encoding

Along the embedding, an input encoding is concatenated and fed to the transformer layer. In natural language processing, the encoding is meant to allow the model to benefit from the sequential information of the words in a sentence. It can be obtained from a sinusoidal function using the position index or simply treated as another learnable parameter. The sequential relations are not present in the jet data, because all the jets originate from the same proton-proton collision, hence, the latter approach is used in this project. It is worth mentioning, that from empirical analysis, the learnable encodings have a significant impact on the final results as they represent a trained, hidden state concatenated to all inputs during evaluation, as shown in equation 3.2. Its impact is especially prevalent for the HLF data (where $L = 1$), where the hidden state matched input's dimension and effectively doubles it after concatenation.

$$\text{encoding}(\hat{\boldsymbol{x}}^{\boldsymbol{i}}{}_{\text{emb}}) = w_{\text{encoding}} \in \mathbb{R}^{1\times d} \implies \text{concat}(\hat{\boldsymbol{x}}^{\boldsymbol{i}}{}_{\text{emb}},\ w_{\text{encoding}}) \in \mathbb{R}^{(L+1)\times d} \tag{3.2}$$

Choosing a learned hidden state is also more efficient for inference in hardware, as the increased training cost associated with back-propagation of this parameter yields a constant set of values that are known during compile-time of the FPGA and can be implemented using a LUT.

3.1.3 Normalization and Parameter Extraction

As layer normalization does not track and gather running mean and variance statistics, this mechanism is implemented on top of the existing `PyTorch` implementation to facilitate extracting the aggregated statistics after training. These, along with all the learned weights and biases, are extracted and transformed into specific C++ formats supported in HLS using a custom tool developed for this purpose. This allows for directly initializing the FPGA's BRAMs and LUTs with the model parameters, which avoids the need for an interaction with a host machine.

Obtaining the statistics taken for the data before normalization layers can also be viewed as a hardware-aware optimization. This can be explained with the mathematical derivation presented in equation 3.3

$$y = \frac{x - E[x]}{\sqrt{Var[x] + \epsilon}} \cdot \gamma + \beta = x \cdot \left(\frac{\gamma}{\sqrt{Var + \epsilon}}\right) + \left(\beta - \frac{\gamma * E}{\sqrt{Var + \epsilon}}\right) = w \cdot x + b \tag{3.3}$$

By treating the mean $E[x]$ and variance $Var[x]$ of input x as learned parameters, the square root and division operations can be fully omitted by fusing them into the existing γ and β parameters which simplifies the hardware required for the normalization layers. This is especially useful as

FPGAs lack dedicated hardware for these computationally expensive operations, which could lead to suboptimal designs being synthesized. Independently of the implementation in this work, a similar idea has been proposed and successfully used as an optimization in the past [56].

The algorithm behind the parameter extraction is rather simple, and the difficulty comes from the domain specific knowledge of handling `PyTorch` model parameters and generating the correct files for HLS. The break-down of the necessary steps can be seen in algorithm 3.1.

Algorithm 3.1 Mechanism behind model parameter extraction

```
state ←load_state(model)
sort(state)
curr_weight ←null
for param in state do
    mean ←find_mean(model, param)
    var ←find_var(model, param)
    if param is weight then
        curr_weight ←param
        new_param ←update_weight(param, var)
    else
        new_param ←update_bias(param, curr_weight, mean, var)
    end if
    save(new_param)
end for
```

3.2 Ultra-Low Latency Architecture

The first of the proposed architectures targets the HLF representation dataset, where each sample is of $\mathbb{R}^{1\times16}$ dimensions, making it a better candidate for an N times faster inference than the constituent list representation with inputs with $\mathbb{R}^{N\times16}$ dimensions. The simpler data means that the network can achieve satisfactory classification results with a lower learning capacity, hence allowing for various simplifications of the base architecture.

3.2.1 Optimization and Tuning

The hypothesis leading the optimization process is that the HLF dataset can be learned by a relatively lower complexity network. The strategy is to start with the accuracy and AUC value of the base architecture and keep applying changes to the network as long as they do lead to significant drops in classification results, with detailed evaluation discussed in chapter 5. Doing so is inherently beneficial for the later FPGA mapping, as even without hardware-aware changes, a simpler model is likely to require fewer resources and achieve lower latency.

The architecture features that have the highest influence on the overall performance are the size of the latent dimension and number of transformer layer. In the case of the original transformer model [32], 12 transformer layers are used, split equally into a decoder and encoder parts of the networks. This, along with latent dimension size of 512 shows that jet tagging requires significantly less complexity compared to natural language processing, as the recent ConstituentNet [8] is based on only 3 transformer layers and embedded dimension of 64. However, as the latter network targets a more complex dataset, the first optimization performed in this project yielded a reduction to only a single transformer layer with latent size of 16. The network complexity is directly proportional to the number of layers, while the self-attention complexities shown in section 2.2.6 can be simplified given the dimensions of *queries*, *keys*, and *values* are shared and equal to $\in \mathbb{R}^{N\times d}$ in this work, as shown in equation 3.4 and 3.5 for time and space respectively. It is worth mentioning that the shared dimension d is purposefully represented this way as it is equal to the model embedded dimension d.

$$\mathcal{O}(h\cdot(N_Q N_K(d_Q+d_V)+d_Q^2(N_Q+N_K)+d_V^2 N_K+N_Q d_V d_{out}))\equiv\mathcal{O}(hNd(N+d+d_{out}))) \quad (3.4)$$

$$\mathcal{O}(h \cdot (N_Q(N_K + d_V) + d_Q(N_Q + N_K) + d_V N_K + N_Q d_{out}))) \equiv \mathcal{O}(hN(N + d + d_{out}))) \quad (3.5)$$

Another successful optimization was simplifying the SiLU to ReLU activations, as in hardware, the latter rely on a single comparator to determine whether to pass input to output directly or set the signal to zero. In contrary, SiLU requires computing the sigmoid function as well as performing a multiplication, which has a non-trivial cost on an FPGA.

Interestingly, the layer normalization was first changed to batch normalization to simplify the tracking and embedding the running data statistics. This only leads to a marginal accuracy decrease, however, it is interesting to point out that so does removing the normalization layers from the design. This can be attributed to the "smoother" distribution of elements of the normalized HLF dataset, which tend to average around zero instead of taking values from a wide range as it is the case for the constituent list representation, shown in figure TODO. Hence, the used dataset does not benefit from additional normalization, vastly simplifying the architecture.

Simple visualization of the distribution in HLF and constituent list

3.2.2 Summary

The optimizations described in the previous subsection correspond to a noticeably simpler architecture, which can be seen in figure 3.2. It is also worth mentioning that the simplifications targeted the components of the transformer block other than the multi-head self-attention block. This is a result of the used mechanism's key role in the learning process as well as the fact that it is difficult to modify it as it uses very basic components, and changing them would impact the underlying, commonly-approved function.

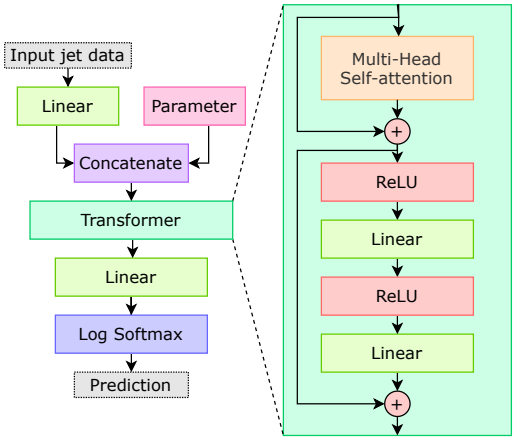

Figure 3.2: Diagram with an overview of the ultra-low latency architecture.

3.3 Accuracy-Focused Architecture

The aim of the second architecture is to exploit a bigger design along with the more complex constituent list dataset to achieve a higher accuracy and AUC value that the ultra-low latency

model while still meeting the latency constraints of L1T at LHC. In addition, this design undergoes a design space exploration to compare and reason about a number of existing and novel techniques.

3.3.1 Optimization and Tuning

Aside from the increase in computational complexity, the biggest difference caused by changing the datasets is the vastly different range and distribution of samples, showcased in figure TODO. While the network could perform normalization as its first layer, this approach was tested to significantly degrade the results quality. This is likely due to the fact that each samples' feature follows a distinct distribution and lays within a different range, so normalizing causes a loss in the carried information. These distributions can be seen in figure TODO.

Maybe claim visual differences between distributions of HLF and constituent list

Normalization and data distribution also need to be discussed for a different reason in the context of this architecture. The layer normalization layers present in the base design are not completely omitted this time, and instead changed to batch normalization. Although the layer normalization characteristic of not tracking running statistics and relying on per-layer normalization during evaluation can yield improvement to classification results, it is not a desired behavior for FPGA mapping due to the lack of hardware support for the square root and division operations. This could be resolved in an analogous way to batch norm by simply manually tracking the statistics, but this was experimentally proven to substantially affect the accuracy. What is more, the less clustered and more diverse distributions of constituent list dataset features lead to numerical instability in softmax calculations of the exponential function. Even though this was a marginal issue for the PyTorch implementation, it was quickly observed to drastically change the expected outcome of the early HLS prototype implementations. A solution to this issue lays in using additional normalization layers just before the self-attention softmax blocks, which not only solved this problem, but also very slightly increased the learning capacity of the network.

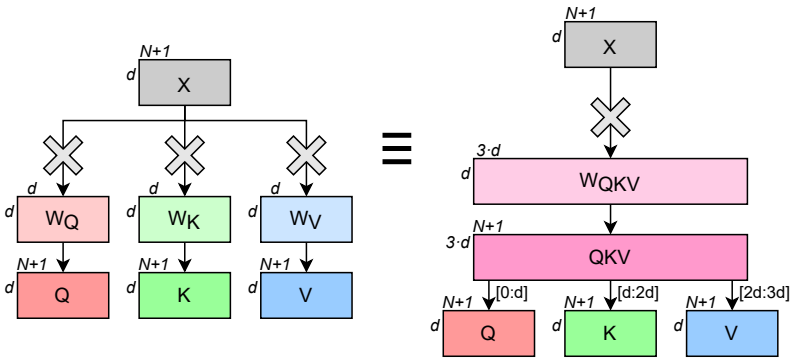

Figure 3.3: Simple illustration for equivalency between matrix multiplication using merged and unmerged weights on the example of *queries*, *keys*, and *values* used in self-attention.

It is a common for GPU training to merge together adequately shaped fully-connected layers, as seen in figure 3.3. This allows the GPU to more optimally use its resources for the computation, potentially decreasing the training time without affecting the results. Nonetheless, this approach was dropped for this architecture to avoid generating one bigger weight matrix in favor of several smaller ones. Contrary to GPUs, the synthesis process for FPGAs benefits from smaller precomputed matrices as it is easier for the algorithm the map them to certain BRAMs or LUTs that are close to the components that read from or write to them. With the significantly smaller dimension sizes for the ultra-low latency model, this aspect generated negligible difference, while in this architecture the merged weight matrix size would exceed a reasonable size and lead to an extremely long synthesis process and likely suboptimal hardware mapping.

Lastly, some optimizations are inherited from the ultra-low latency architecture. The SiLU are replaced by ReLU activations, while embedding and encoding are simply implemented by a fully-connected layer and a learnable parameter. When it comes to the transformer layer count and

latent dimension size, they follow the configuration of ConstituentNet of 3 and 64, however, a closer evaluation and discussion about these are carried in chapter 5.

3.3.2 Summary

In this case, the resulting architecture is much more similar to the base one in terms of its overall structure, however it differs from it with the crucial changes to normalization layers, activation function and modifications to the multi-head self-attention block. The overview of this design can be seen in figure 3.4.

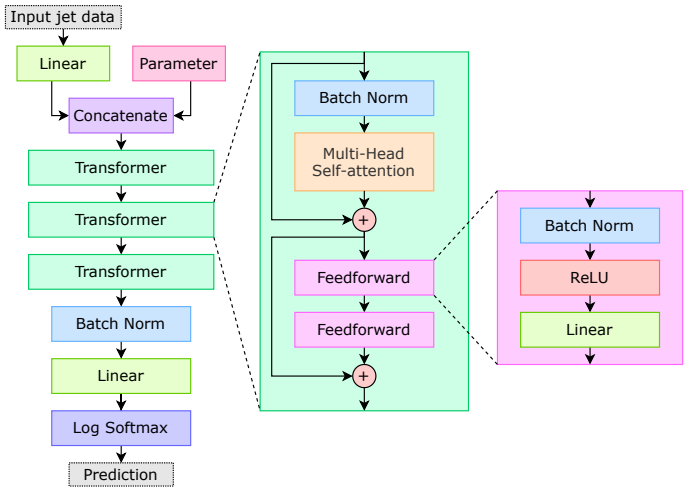

Figure 3.4: Diagram with an overview of the accuracy-focused architecture; the inclusion of batch normalization before softmax within the multi-head self-attention block is not showcased for the sake of clarity.

3.4 Quantization-Aware Training

The use of the term *quantization* in the topic of machine learning and reconfigurable hardware might appear as a misnomer if one follows the definition used in signal processing, where it refers to constraining continuous values to a set of discrete ones. However, this definition can be extended for converting values from a very large set of discrete values to a significantly smaller ones. This is the case when half (16 bits), single (32 bits) or double (64 bits) precision floating-point numbers are expressed using a fixed-point representation. This leads to an inherent quantization noise because many distinct values in floating-point representation map to the same number when stored as fixed-point, which can be seen in figure 3.5 [57]. Although this work exploits fixed-point arithmetic for its efficient hardware representation, it has to be noted that quantizing is also used for time and space efficient GPU inference as it can vastly lower the total bits used across model's weights, hence reducing the required memory and computational complexity.

3.4.1 Floating-point and Fixed-point Representations

To bring more perspective to this topic, let's start by observing the 16-bit wide floating-point notation with an example seen in equation 3.6. *SIGN*, *EXP* and *FRAC* stand for the sign, exponent and fractional[1] fields (sequences of 1's and 0's) of a number.

$$\{\text{SIGN} \mid \text{EXP} \mid \text{FRAC}\} = \begin{cases} (-1)^{\text{SIGN}} \cdot 2^{-14} \cdot (0.\text{FRAC}_2) & \text{EXP} = 00\_000_2 \\ (-1)^{\text{SIGN}} \cdot 2^{\text{EXP}-15} \cdot (1.\text{FRAC}_2) & \text{EXP} \in [00\_000_2,\ 11\_110_2] \\ \pm\infty & \text{EXP} = 11\_111_2 \end{cases} \tag{3.6}$$

[1] Also referred to as *significand precision*

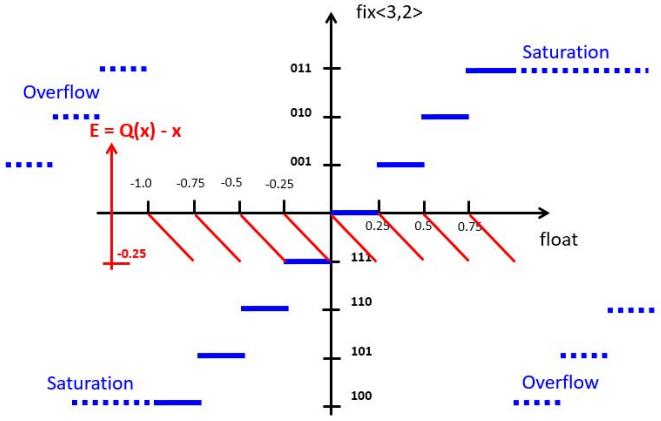

Figure 3.5: Quantization noise from 32-bit floating-point to 3-bit (2-bit integer, 1-bit fractional) fixed-point representation; widths selected to highlight the behavior. Two methods of handling values outside representable range are showed: classic overflow as well as saturation to minimum or maximum value.

The widths of the fields for standard floating-point width can be seen in table 3.1, however, the particular details in the example do not need to be fully understood to notice the required complexity of the hardware design to perform operations using floating-point values. It has to first decode each of the fields, check for special values, normalize inputs to a common base, perform the computation, and lastly normalize again and decode the fields. As it can be expected, this comes with a significant overhead compared to integer numbers.

Table 3.1: Comparison of standard precision types for floating-point values. Note the difference in half precisions, where *Brain* offers same the exponent width as single precision, and *binary* priorities fractional precision.

Precision	**Total width**	**Field width**		
		sign	exponent	fractional
Double	64	1	11	52
Single	32	1	8	23
Half (*Brain*)	16	1	8	7
Half (*binary*)	16	1	5	10

While dedicated circuits exits in CPUs and GPUs to accelerate floating-point calculations, FPGAs tend to use fixed-point representation to achieve superior latency with relatively simple hardware resources. It comprises a sequence of P binary digits representing the integer part, then a virtual decimal point, followed by R binary digits representing the fractional part, according to equation 3.7.

$$\{I_{P-1}|...|I_0|F_{R-1}|...|F_0\} = I_{P-1} \cdot 2^{P-1} + ... + I_0 \cdot 2^0 + F_{R-1} \cdot 2^{-1} + ... + F_0 \cdot 2^{-R} \tag{3.7}$$

The virtual decimal point is not explicitly present in the number, instead the lengths of the sequences are stored which allows for correct handling. There are also no widely adopted standards for the internal widths of fixed-point numbers, as they are often implementation-specific. Fixed-point hardware is only responsible for correctly aligning the inputs in case they vary in width, which is an information know at compile-time, as opposed to run-time for floating-point numbers, which makes it very suitable for FPGAs.

3.4.2 Existing Implementations

Quantization-aware training refers to training a model using the fixed-point representation of numbers to allow the model to reduce the impact of the quantization noise by learning the underlying

data characteristics with less precision. However, approaches differ in the degree to which the quantization is used as it can be applied to training data, weights and biases, intermediate results or any combination of these. It also has to be noted that existing implementations have been designed with different objectives, although to the best of our knowledge, the most widely used ones are still in their very experimental phases at the time of writing this report. The approaches considered for this work are listed below:

- **PyTorch Eager Mode Quantization** [58] - currently in a *beta* version. PyTorch offers two development modes - Eager, for research purposes and easier experimentation, as well as Script, for production use cases [59]. This quantization scheme is an extension to the former mode and requires manual handling of the placement of quantizing and dequantizing layers in a network as well as operator fusion and functional blocks. Currently, offers no support for the vanilla recurrent block, LSTM, GRU or self-attention.
- **PyTorch FX Graph Mode Quantization** [60] - similarly to the previous point, it is in a *prototype* version, and it extends the graph-base and speed-focused Script mode. This leads to an easier implementation as the quantization feature support process happens automatically. It does not work for convolutional, self-attention or embedding layers yet.
- **Brevitas** [61] - a research project from a team at Xilinx, a major reconfigurable hardware vendor. It is early in its development cycle, but it promises to support most network architectures, provided that all existing layers are replaced with their quantized variants, and quantizing and dequantizing is also handled manually, similarly to PyTorch Eager Mode Quantization. Its caveat is that while it provides a granular, per-variable level of bit-width customization, the offered fixed-point widths cannot be easily changed in size.
- **QPyTorch** [62] - a Cornell University research project, which offers a fixed-point simulation framework. Existing networks can be easily adapted to it, only requiring manual quantization layers usage throughout the design. These can be of arbitrary width, which supports a rich design space exploration, however, the representation of widths, biases, accumulators and gradients needs to follow the same quantization scheme for all layers, which is dictated my the training optimizer configuration.

It is clear that each described solution comes with its own advantages and disadvantages. Even though the first two approaches come officially from PyTorch, they lack support for the core transformer layer - the self-attention. Hence, this report proposes the latter two for research on quantized transformer architectures and their hardware implementations.

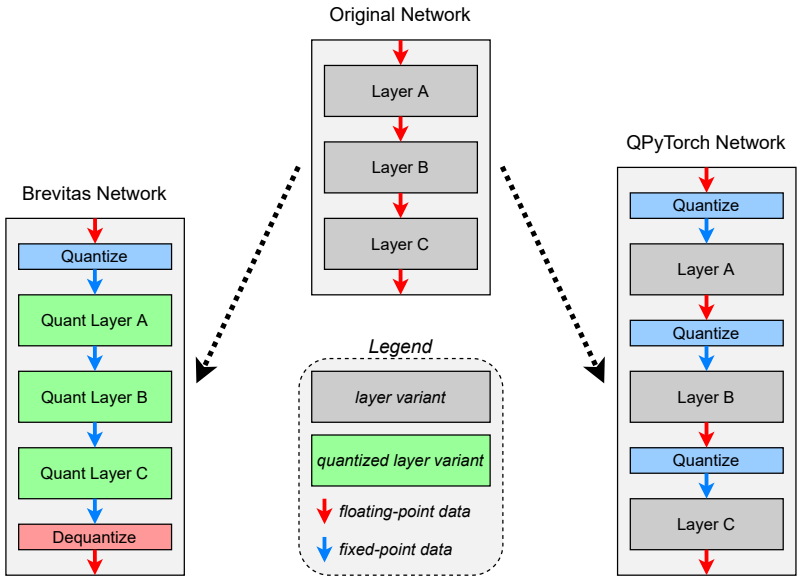

Figure 3.6: Comparison of a simple neural network prepared for quantization-aware training using Brevitas and QPyTorch frameworks.

Figure 3.6 showcases the designs resulting from quantizing a simple neural network using Brevitas and QPyTorch. The former approach relies on library-provided quantized variants of commonly found neural layers, and each can have its input's, output's and internal parameters' bit-width configured separately to one of the pre-defined types. This technique is more truthful to how FPGAs operate, but at the same time, more demanding in terms of implementation complexity than QPyTorch's one, which exploits the wide range of PyTorch's native layers and only requires custom quantizing blocks in between them. The latter is also slightly less computationally intensive, however both methods results in significantly longer training time than the floating-point representation due to the lack of support for fine-tuned, fixed-point GPU implementation of the network layers. It is also worth mentioning, that Brevitas offers a convenient way of exporting the quantized models to Xilinx hardware representations as well as external tool chains. Lastly, quantization is also proposed and discussed as a post-training mechanism in section 4.4, with both approaches then evaluated and compared in chapter 5.

Chapter 4

Hardware-Aware Analysis

In this chapter, the hardware-aware optimizations used in the FPGA implementations are first presented and then their application in the proposed architectures is explained. Other elements of the hardware design and configuration process are then described which results in a comprehensive picture of the FPGA-mapped architectures. Afterwards, two analytical models are considered - one for the latency and the other for the resource utilization. The custom post-training quantization tool is discussed along with its suitability for this project. Then, existing infrastructure that ties together higher and lower-level code representation is introduced along with its synergy with a High-Level Synthesis optimization tool chain. Lastly, the technical contributions to `hls4ml` library are listed and explained.

4.1 Hardware-Aware Optimizations

4.1.1 Tensor Multiplication and Scaling

Each self-attention head performs two tensor multiplications (referred to as *matmul* blocks in figure 2.4), which are normally expressed using Einstein Summation notation [63], which is supported by mathematical and machine learning libraries like `NumPy` or `PyTorch`. However, not present by default in HLS, it requires careful design of the calculation loops in order to not cripple the performance by unnecessary computations and pseudo-random data accesses. As part of this research, an efficient and fully-customizable HLS block has been designed, that uses a very similar interface to the Python equivalent.

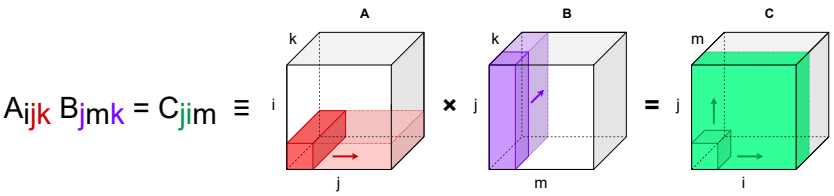

Figure 4.1: Visualization of a tensor operation expressed in Einstein Summation notation.

Figure 4.1 shows a visualization for an example notation to give a better understanding of the necessary flexibility of a formula. The translation between notations using the custom tool is showcased in listing 4.1. While the `PyTorch` implementation can often use 4-dimensional tensors, the first dimension refers to the batch, which is not present in the hardware implementation that processes input samples one-by-one, hence both the figure and code listing show 3-dimensional cases. It is also worth pointing out, that tensor multiplication is an inherently computationally expensive operation due to the quadruple-nested loop structure. For this reason, the proposed design leaves the configuration of pipelining as a parameter that offers a trade-off between time and design complexity. The *design* complexity refers to the difficulty involved in HLS synthesis as well as hardware resource utilization. In other words, the hardware block can be instantiated

to run serially, where little resources are needed as they get re-used, or alternatively, in parallel, where significantly more components are used to decrease latency, and in case the design is also pipelined, to also increase throughput.

```
#define EINSUM_PIPELINE(DEPTH) {\
  if (io_type == io_parallel) {\
    if (pipeline_einsum_depth == DEPTH) {\
      #pragma HLS PIPELINE II=reuse_factor\
    } else {\
      #pragma HLS unroll \
    }}}

type_t out[H][K][Q];
if (io_type == io_serial) {
  #pragma HLS ARRAY_PARTITION variable=out cyclic factor=cycle_factor
} else if (io_type == io_parallel) {
  #pragma HLS ARRAY_PARTITION variable=out complete
}

Einsum_H: for (unsigned hh = 0; hh < H; hh++) {
  EINSUM_PIPELINE(3);
  Einsum_K: for (unsigned kk = 0; kk < K; kk++) {
    EINSUM_PIPELINE(2);
    Einsum_Q: for (unsigned qq = 0; qq < Q; qq++) {
      EINSUM_PIPELINE(1);
      Einsum_C: for (unsigned cc = 0; cc < C; cc++) {
        EINSUM_PIPELINE(0);
        if (cc == 0) out[hh][kk][qq] = 0;
        out[hh][kk][qq] += A[qq][hh][cc] * B[kk][hh][cc];}}}}
```

List of Listings 4.1: From PyTorch `out = torch.einsum("qhc,khc->hqk", [A, B])` to HLS C++ code.

$$\text{Design} : \mathcal{O}(n) \quad \text{Time} : \mathcal{O}(HKQC \cdot n) \tag{4.1}$$

Let's consider the two extreme cases for the design - no loop unrolling and complete unrolling, where the latter is required for the block to be fully pipelined, and assume that multiply-accumulate and addition both have n time and space complexity. In the first case, a single multiply-accumulate operation happens at once, hence a final result is only available after all the loops have been fully iterated, with complexities shown in 4.1.

$$\text{Design} : \mathcal{O}(HKQC \cdot n) \quad \text{Time} : \mathcal{O}(n \cdot \log(HKQC)) \tag{4.2}$$

In the second one, all loop operations can execute at the same time, although the intermediate results need to be summed accordingly using an adder tree (seen in figure 4.2) which has a logarithmic time and linear space complexity, before saving the output tensor, which leads to complexities seen in 4.2. The time complexity may appear high, but it has to be remembered that unrolling allows for the pipelining of this design, which cannot decrease latency, but can vastly increase throughput, as each addition can happen in a single cycle.

Another simple optimization used alongside the tensor multiplication blocks was the change in size scaling from using division to performing an arithmetic right shift (ASR), which requires precomputing the logarithm of the size, seen in equation 4.3, vastly simplifying the otherwise computationally expensive hardware required at run-time.

$$\frac{x}{\sqrt{\text{size}}} \equiv \text{ASR}(x,\ \log_2 \sqrt{\text{size}}) \equiv \text{ASR}(x,\ \frac{1}{2} \log_2 \text{size}) \tag{4.3}$$

4.1.2 Softmax and Log Softmax Activations

Despite an already existing `hls4ml` implementation of the softmax activation function, computing the logarithm of its result is not as simple as it may seem. This is because the numerical stability and computational efficiency of this operation is often explored in-depth [64] and varies depending on the programming language and target platform.

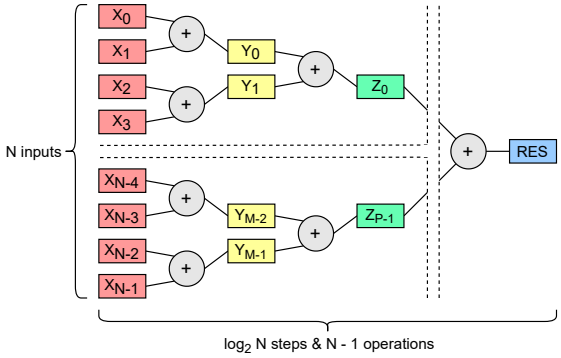

Figure 4.2: Illustration of an adder tree with N inputs.

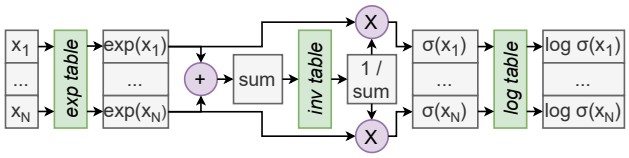

Figure 4.3: Direct hardware implementations of log softmax.

The naive implementation comes straight from the definition of taking a logarithm of softmax, seen in equation 4.4, and the required hardware operations are shown in figure 4.3.

$$\sigma(x_i) = e^{x_i} / \sum_{j=1}^{N} e^{x_j} \tag{4.4}$$

This report proposes a different way of mapping this operation to hardware to improve stability while shortening the critical path and using less resources. It is based on the derivation shown in equation 4.5.

$$\log(\sigma(x_i)) = log(e^{x_i} / \sum_{j=1}^{N} e^{x_j}) = \log(e^{x_i}) - \log(\sum_{j=1}^{N} e^{x_j}) = e^{x_i} - \log(\sum_{j=1}^{N} e^{x_j}) \tag{4.5}$$

The resulting hardware operations are depicted in figure 4.4. It is important to note, that operations like exponentiation, division or taking a logarithm usually rely on precomputing a wide range of values and mapping them in BRAMs or LUTs to allow for lookup on run-time. Hence, the optimized design requires one less of such lookups while also replacing multiplication by a subtraction, which can be simpler to express in hardware.

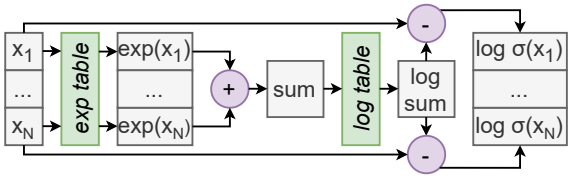

Figure 4.4: Optimized hardware implementations of log softmax.

Confirm if page breaks correctly.

Although further simplifications, including approximating the summation by finding the maximum (see equation 4.6) or simply omitting the logarithm portion of the expression, were also explored, they noticeably lowered the final accuracy and were thus abandoned.

$$\log(\sigma(x_i)) = e^{x_i} - \log(\sum_{j=1}^{N} e^{x_j}) = e^{x_i} - \sum_{j=1}^{N} \log(e^{x_j}) = e^{x_i} - \sum_{j=1}^{N} x_j \approx e^{x_i} - \max(x) \tag{4.6}$$

4.2 Neural Network Architectures Design

4.2.1 Ultra-Low Latency Architecture

4.2.2 Accuracy-Focused Architecture

4.3 Analytical Latency and Resource Models

Reason about computational complexity, include a diagram of self-attention tensor multiplications based on contents of Deep Learning lectures

Derive simple latency and resource (likely only DSP as others are too difficult) model, that will be verified in evaluation chapter

4.4 Post-training Quantization

This section returns to the topic of quantization, but as opposed to section 3.4, it explores the quantization of already trained models. This is domain is not researched as much as quantization-aware training due to the lack of ability for a model to *compensate* for the quantization noise during training, hence leading to potentially inferior results. However, recent advancements in this field [65] leverage the synergy between post-training quantization and the target hardware platform to produce results with improved latency or energy consumption. The inherent noise issues are offset by a careful per-variable bit-width analysis, driven by a reinforcement learning algorithm. The choice of the algorithm has a deep-rooted issue for more computationally demanding models that also require a search in a wider range of bit-widths[1].

4.4.1 Motivation

This report proposes a novel post-training quantization algorithm that can be applied to state-of-the-art transformer neural networks over a wide precision range. Early tests in the HLS environment revealed that a single C simulation for an input with only 100 samples can take around 10 minutes, which dictates a need for a significantly simpler, hence faster, algorithm than Bayesian optimization or reinforcement learning to allow for an exploration that runs in a reasonable amount of time.

The motivation of the algorithm comes from a hypothesis which states that the neighboring layers in a neural network have a relatively high correlation in their optimal bit-widths. Under this assumption, each layer's input, output, weight, bias and accumulator can be safely explored one-by-one, in the order of appearance in the model. *Safely* refers here to a low likelihood of arriving at a local accuracy extremum that is substantially worse than the global one, that could only theoretically be found using a more sophisticated approach. During this *walk* through the design space, several non-trivial constraints about the widths have to be ensured, which are the topic of the next subsection.

4.4.2 Constraints

The constraints of a network variable could theoretically be set arbitrarily to convey a high-level requirement of an experienced designer with a knowledge about typical widths used for a component in a given network type. However, the proposed method automates this process by extracting the underlying lookup table characteristics to accommodate users without domain-specific expertise. These characteristics are part of the network configuration that ensures that any precomputed (for increased latency) function is stored with adequate precision that avoids introducing unnecessary errors. To give a more concrete example to this abstract definition, one can consider the range of

[1] The mentioned method only explores convolutional neural networks in $[1, 8]$ bit-width range.

values yielded from the exponential function. Not only is there a set width for the results, but even relatively small values map to numbers that require several bits of integer precision, so careless reduction to either of the width parts can quickly degrade any learning capacity of the model.

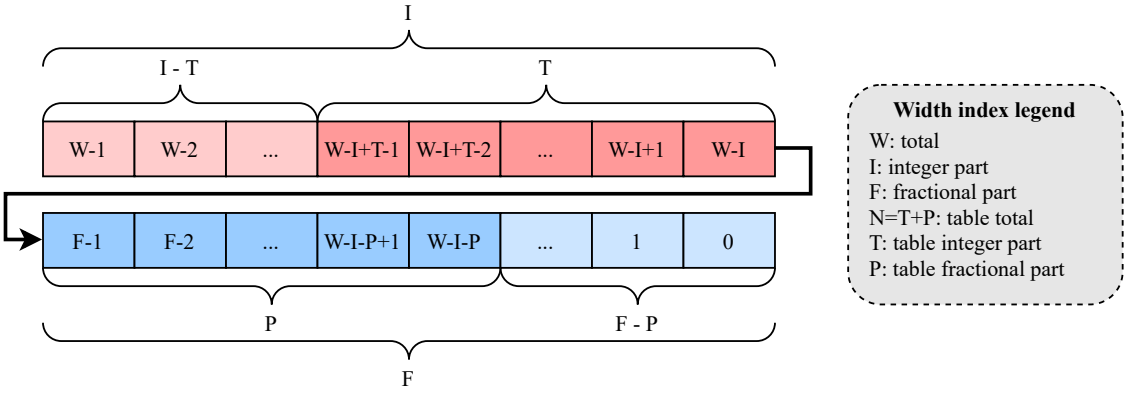

Figure 4.5: Visualization of a fixed-point number with its bit-widths as well as constraints imposed by a lookup table. For convenience, red and blue distinguish integer and fractional parts, while the darker hue shows the table-related parts.

Figure 4.5 visualizes a fixed-point number with a detailed analysis of its structure in terms of lookup table constraints, which were added as an optional feature, and are described in section 4.6.3. At first, it could be assumed that the imposed widths should simply be adopted by the variables used by the corresponding table values. However, it is possible for such variables to also have connections to other paths in a network, which can require more precision than the table, hence justifying the existence of the constraints ranges presented in equations 4.7, 4.8, and 4.9, with the notation coming from the corresponding figure.

$$W \geqslant N > T \geqslant 1 \tag{4.7}$$

$$W \geqslant I \geqslant T \geqslant 1 \tag{4.8}$$

$$W \geqslant F \geqslant P \geqslant 1 \tag{4.9}$$

4.4.3 Steps

A high-level overview of the steps used in the proposed method is depicted in algorithm 4.2. The only required parameters are the negative and positive accuracy tolerance, which are used to guide the search process. Increasing the negative tolerance relaxes the accuracy constraints ensured after each algorithm step in order to significantly reduce the overall bit-widths. On the other hand, a complete opposite objective can also be achieved as reducing the positive tolerance priorities quality of results over narrower bit-widths. Overall, these parameters can take an arbitrary combination of non-negative values that best expresses the exploration goals.

The algorithm starts by scanning an HLS file that includes all the fixed-point types used in a model, convert them into objects and organizes them into a First In, First Out (FIFO) queue, according to their original order. One by one, objects are popped from the queue and undergo the search process. Firstly, the bit-width that was found in the file is saved, the object inherits from the previous optimal bit-width (based on the correlation hypothesis), and the model is evaluated. Depending on whether the results stay within the accuracy tolerance, the object starts with either its original or the inherited configuration. Afterwards, the integer and fractional parts go through one or two loops - first, at each iteration the width gets incremented as long as it matches the target range. After the first loop, the second one, analogous but checking designs with fewer bits, is only entered if no significant improvements were found when increasing widths. This avoids evaluating same configurations unnecessarily, which goes in line with the overall aim to offer a relatively quickly-converging solution to the very multidimensional optimization problem. Once

all width objects reach their optimal state, the found configuration is saved and can be used in a further design space exploration.

It is important to point out that the aforementioned PyTorch Eager Mode and FX Graph Mode quantization schemes offer post-training quantization, but there are unsuitable for this work due to their lack of flexibility and support for the essential neural network layers. Instead, the HLS source directory is modified and tested in a C Simulation to measure accuracy. While the synthesis process could supplement the algorithm with an additional feedback signal about the precise hardware resource utilization, it takes much more than the simulation, and its results can be estimated to vary linearly with the total number of bit-widths. The only situation when such assumption does not hold is when a hardware component input width limit is reached because then a 1-bit increase requires an additional instance of that component to be instantiated. Ways of avoiding this issue are covered along with the evaluation of the results in section 5.3.2.

4.5 High-Level-Synthesis Optimization

Introduce MLIR and the overall flow of how PyTorch models are mapped, include nice diagrams

|

|

|

|

|

Talk about how ScaleHLS extends MLIR to HLS, again diagrams

|

|

|

|

|

Talk about potential integration/relation between hls4ml (Python -> HLS) and ScaleHLS (PyTorch/HLS -> Optimized HLS)

|

|

4.6 `hls4ml` Contributions

In this section, the technical contributions to the `hls4ml` library are descriptively presented, highlighting the areas that this work expands upon. Developed components are shown in figure 4.6, along with a number of existing components that were expanded upon or are used to draw comparison with. Each group is discussed in one of the following subsections, in an order of increasing design complexity.

Algorithm 4.2 Algorithm for performing post-training quantization search

```
function PostTrainingQuantization(neg_accuracy_tolerance, pos_accuracy_tolerance)
    previous_width ← null
    max_decrement ← neg_accuracy_tolerance · 2        ▷ Maximum decrement per parameter
    optimal_accuracy ← find_accuracy()
    params ← scan_file(defines_file)                  ▷ FIFO with scanned parameter objects
    while params not empty do
        current ← params.pop()
        if previous_width exists then                 ▷ Try using width from previous parameter
            original_width ← params.width
            update(params, previous_width)
            if find_accuracy() < optimal_accuracy − max_decrement then
                update(params, original_width)
            else
                optimal_accuracy ← find_accuracy()
            end if
        end if
        for part in {int, frac} do
            try_increase ← True
            pos_improvement_found ← False
            while try_increase do                     ▷ Increment to check for high accuracy gain
                param.increment(part)
                if find_accuracy() > optimal_accuracy + pos_accuracy_tolerance then
                    optimal_accuracy ← find_accuracy()
                    pos_improvement_found ← True
                else
                    try_increase ← False
                    param.decrement(part)
                end if
            end while
            if not pos_improvement_found then         ▷ Decrement if no good increment
                try_decrease ← True
                acc_before_decrease ← optimal_accuracy
                while try_increase do
                    param.decrement(part)
                    if acc_before_decrease− find_accuracy()> max_decrement then
                        try_decrease ← False
                        param.increment(part)
                    else if find_accuracy() > optimal_accuracy−neg_accuracy_tolerance then
                        optimal_accuracy ← find_accuracy()
                    else
                        try_decrease ← False
                        param.increment(part)
                    end if
                end while
            end if
        end for
    end while
    return params
end function
```

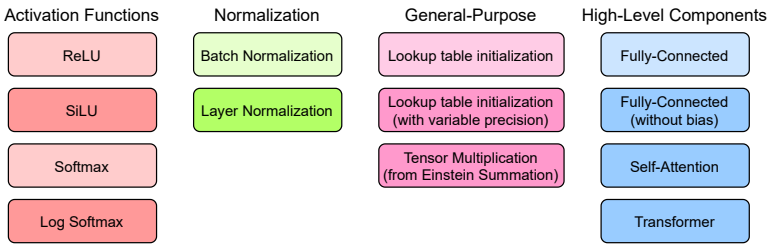

Figure 4.6: Overview of the created implementations (dark-colored) and some existing components with similar functionality (light-colored).

4.6.1 Activation Functions

The library offers several common non-linear activation functions, including the basic one - ReLU. An implementation was created for the SiLU, which extends the existing ReLU block by adding multiplication with the sigmoid function that can happen serially or in parallel depending on the specific configuration. In addition, the log softmax activation had implementations developed using both the direct and the optimized method described earlier in this chapter in section 4.1.2 to be able to evaluate the success of the optimization process.

4.6.2 Normalization Layers

Layer normalization and batch normalization perform the same operation across different dimensions, which on its own would not require a separate implementation. However, they also differ in terms of statistic collection, as only the batch version collects them during training to use during inference while layer normalization always computes them directly. While this is a suboptimal approach for reconfigurable hardware, a simulation-only version of layer normalization was implemented to allow for analyzing the effect of switching between these two methods to better understand their trade-off.

4.6.3 General-Purpose Blocks

The method used in `hls4ml` for mapping the precomputed function values to lookup table indexes prioritizes the integer range of a fixed-point number over its fractional part. In other words, it simply uses the N most significant bits of a value for calculating the table index, where N is the table word width. Although this approach works in the majority of cases, it limits the ease of exploration as the type used in a lookup table might be affected by another variable's width, hence enforcing an unnecessarily wider integer range and sacrificing decimal precision. A good example is the natural logarithm, which output range can be represented using fewer integer bits than its input domain, which makes it the perfect candidate for using the custom lookup table initialization. Aside from that, the tensor multiplication covered in details in section 4.1.1 was implemented in a way to match the style of existing tensor and array modifying components. This makes it very convenient for accelerating more complex designs that rely on Einstein Summation in their PyTorch implementation, and in the future, it could allow `hls4ml` to automatically translate that concept as it is currently not supported.

4.6.4 High-Level Components

It comes as no surprise that `hls4ml` offers a customizable and efficient fully-connected layer implementation. However, the way of creating an instance without the bias calculation is to provide an array filled with zeros. This is believed to be a shortcoming of the current version, as having a compile-time parameter regarding the bias can make the synthesis process faster given that the HLS can skip the optimization process for that aspect. With bigger and more complex models, this simple change could lead to noticeable reduction in processing time. What is more, it also yielded a marginally smaller design in the case of this work, suggesting that the HLS hardware translation might not be behaving optimally, but that depends on a number of factors and was not evaluated further.

Although the deeply covered self-attention and transformer layers could be viewed as specific to the topic of this report, it has to be remembered that they are the state-of-the-art when it comes to a plethora of applications. At the same time, they are incomparably more complex than any other aforementioned components, not only needing them for correct functionality, but also requiring considerable amount of development time to properly integrate and carefully optimize. Hence. they are considered the most important `hls4ml` contributions of this work.

Chapter 5

Evaluation

This chapter starts by evaluating proposed neural network architectures using CPUs and GPUs to find a baseline inference latency, accuracy and AUC values. This information is then compared with the results obtained from simulating and synthesizing the models on reconfigurable hardware. The outcome of the design space exploration includes hardware resource utilization metrics as well as discussion about the Pareto front and applicability in high energy physics environments. Lastly, both the pre-training and post-training quantization are evaluated quantitatively in terms of the trade-off between quality of results and bit-width reduction as well as qualitatively for their ease of adaptation to existing designs.

5.1 Architecture Analysis

Carries on from chapter 3

|

|

|

5.1.1 Existing Solutions

Table 5.1: Summary of networks' inference time, accuracy, Floating-Point Operations Per Second and parameter number for optimal batch sizes, with best values in bold.

Neural network	Inference per batch (ms)	Accuracy / aver. AUC	FLOPS	Parameters
DNN [6]	**1.0 ± 0.2**	0.760 / 0.941	**27 k**	14,725
CNN [6]	57.1 ± 0.5	0.740 / 0.911	400 k	205,525
GRU [6]	23.2 ± 0.6	0.750 / 0.912	46 k	15,575
JEDI-net [6]	121.2 ± 0.4	TODO / 0.959	116 M	33,625
JEDI-net with $\sum O$ [6]	402.0 ± 1.0	TODO / 0.957	458 M	8,767
ConstituentNet-Base [8]	∼773.0	0.818 / **0.966**	1,553 M	289,000
ConstituentNet-Tiny [8]	∼17.0	0.805 / 0.960	13 M	**8,533**

5.1.2 Receiver Operating Characteristic Curves

Baseline ROC and its meaning

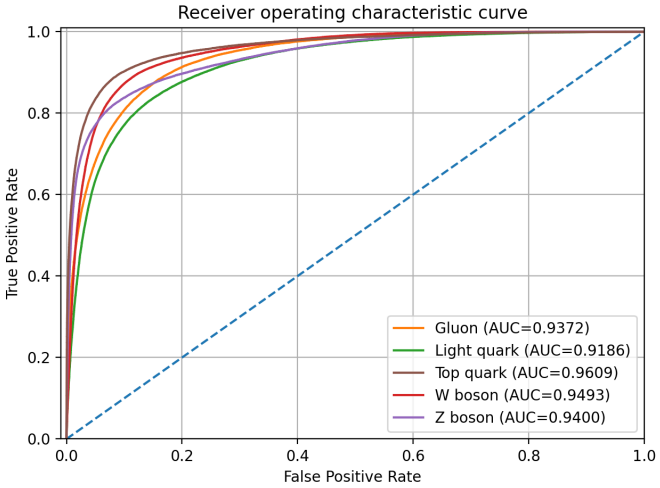

Figure 5.1: ROC curve for TODO

Talk about grid search for accuracy-focused model as a quick and easy hyperparameter search, that was done mainly to look for simpler designs given very long synthesis, not hardcore tuning accuracy

Give estimate of how long is the synthesis and why this is a problem

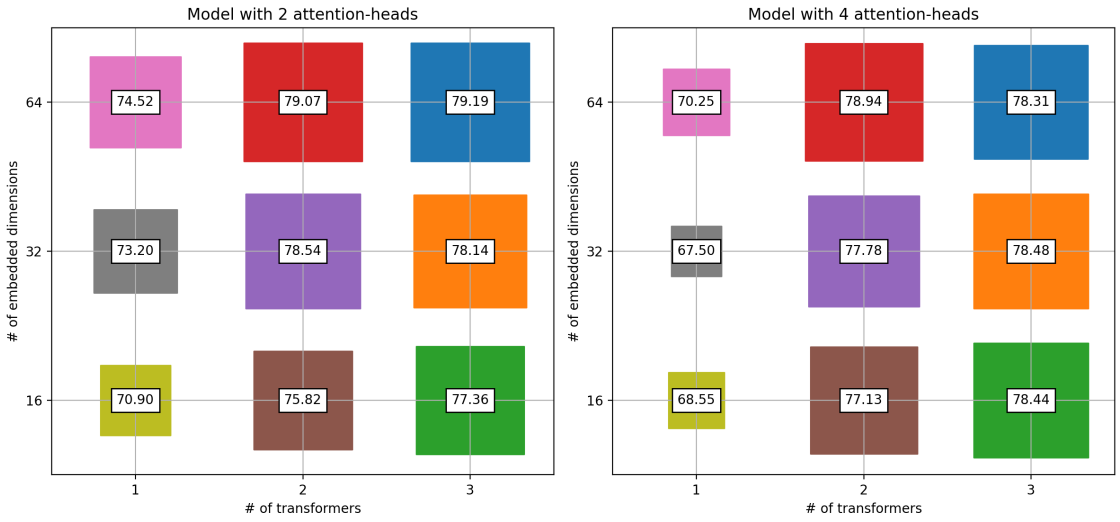

Figure 5.2: Grid-search results - squares area proportional to accuracy.

Ultra-low latency ROC and its meaning

Table with AUC and accuracy

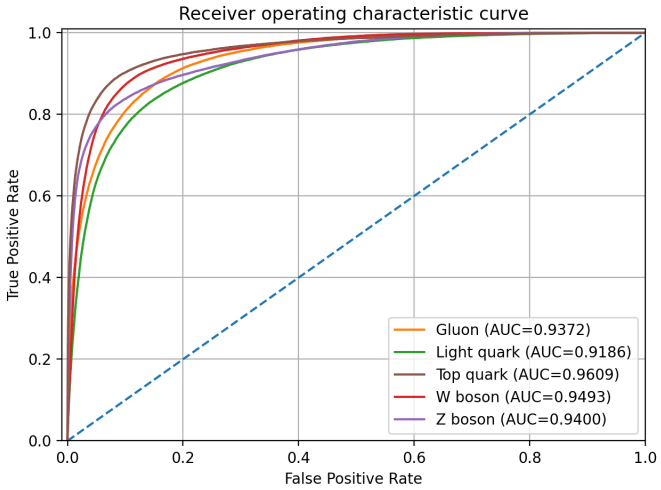

Figure 5.3: ROC curve for TODO

Accuracy-focused ROC and its meaning

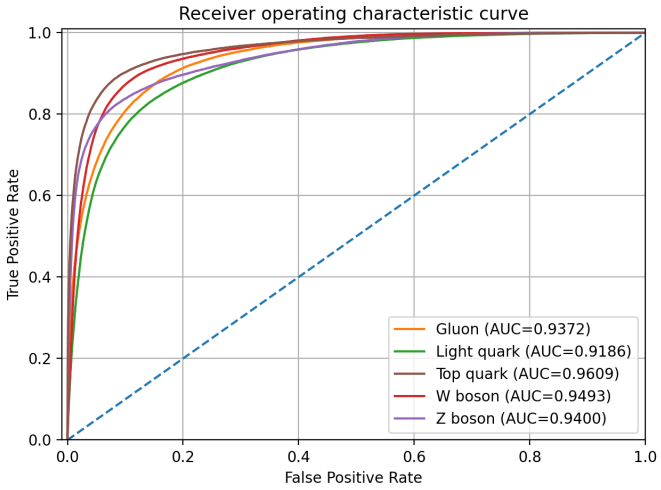

Figure 5.4: ROC curve for TODO

Table with AUC and accuracy

|

|

|

|

5.1.3 Proposed Networks' Latency using CPUs and GPUs

Latency on CPUs and GPUs, extend table below with accuracy-focused latency results or just create a second one

Comment on how little difference there is between all CPUs and GPUs

|

|

The detailed specifications of the machines used for measuring the inference time are listed below. The system specification is shared and includes CentOS 7.0. The first machine that hosts the GPUs has CUDA version 11.5, driver version 495.29.05.

- Dual Intel Xeon Silver 4110 at 2.10GHz with 192 GB DDR4 at 2666 MT/s - GPUs host,
- Dual Intel Xeon X5690 at 3.47GHz with 96 GB DDR3 at 1333 MT/s,
- Intel Xeon E5-2620 v3 at 2.40GHz with 192 GB DDR4 at 2133 MT/s,
- Dual Intel Xeon Gold 6154 CPU at 3.00GHz with 768 GB DDR4 at 2666 MT/s,

Table 5.2: Comparison of simplified model's inference times with batch size of 128

	Device	**Inference time**	
		per batch (ms)	per sample (μs)
CPU	Intel Xeon Silver 4110 (Dual)	1.741 ± 0.027	13.604 ± 0.207
	Intel Xeon X5690 (Dual)	1.622 ± 0.026	12.670 ± 0.206
	Intel Xeon E5-2620 v3	1.325 ± 0.123	10.350 ± 0.963
	Intel Xeon Gold 6154 (Dual)	1.167 ± 0.066	9.112 ± 0.516
GPU	Nvidia GTX 1080 Ti	1.166 ± 0.112	9.111 ± 0.876
	Nvidia TITAN X	1.154 ± 0.119	9.017 ± 0.928
	Nvidia TITAN Xp	1.062 ± 0.036	8.296 ± 0.283

5.2 Hardware Implementation

Small introduction

Thanks to its high-performance, XCU250 (variant figd2104-2L-e) was chosen as the target FPGA platform.

Brief info about XCU250

5.2.1 Ultra-Low Latency Model

Discuss hardware resources and latency

|

Small table with cycles, latency, clock frequency

Table 5.3: FPGA resources utilization

	BRAM 18K	DSP48E	FF	LUT
Total used	12	4,351	58,942	298,881
Available	5,376	12,288	3,456,000	1,728,000
Utilization	0.22%	35.41%	1.71%	17.30%

Explain which and how the design changes affected the results below

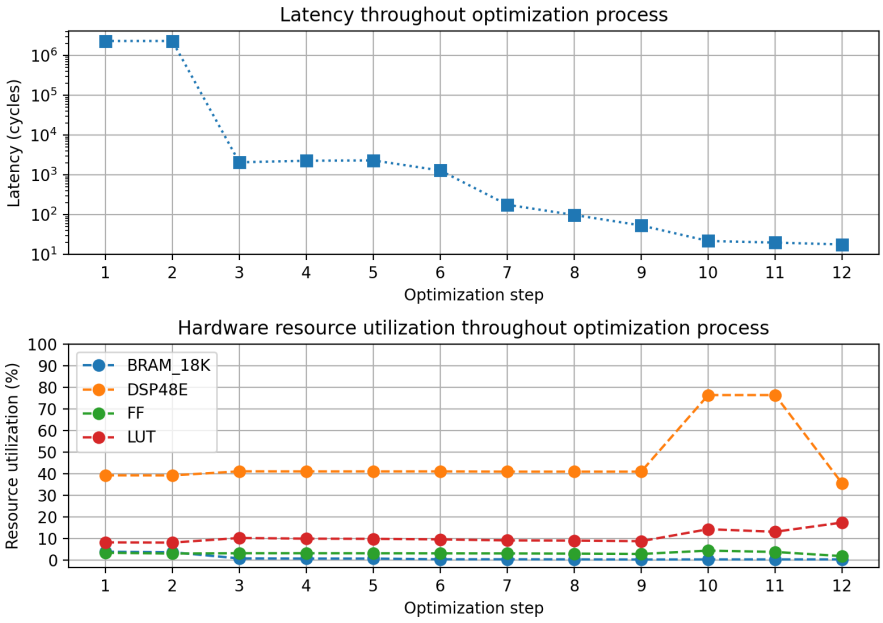

Figure 5.5: Results of the optimization process for the ultra-low latency model.

Talk about Pareto front and its meaning, maybe use a roofline model if it makes sense

|

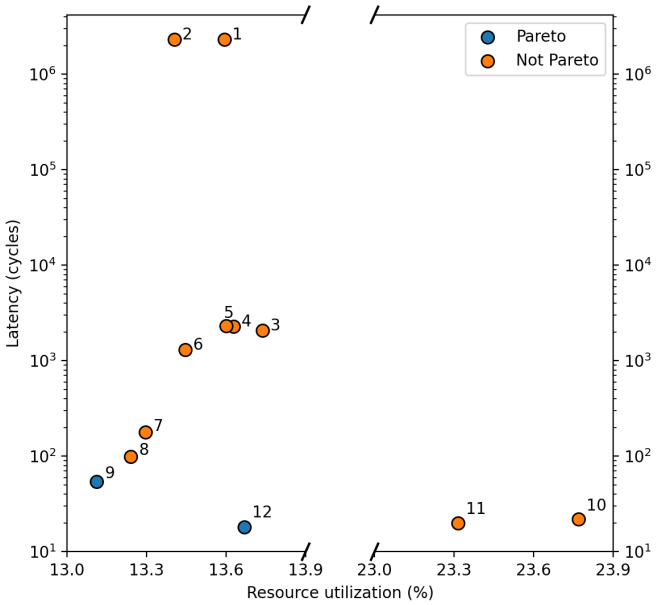

Figure 5.6: Latency plotted against average resource utilization for the ultra-low latency model configurations.

Verify analytical models for latency/resources

5.3 Quantization Results

5.3.1 Pre-Training Quantization

Recap how this was done and talk about results

Mention float16 doesnt learn anything (acc 20%) as its range is too small, and we cannot consider normalizing inputs as its real time system

Mention problems with fixed-point 32 and reason about both int and frac range being important, give examples at which point which one causes issues (likely input -> int range, after normalization -> frac range)

Mention brevitas only gets 34% accuracy and why this is the case and how it could be solved

|

|

|

5.3.2 Post-Training Quantization

State that the results are very promising (64% bits reduction), how this should influence synthesis

prove correlation with how different on average is the next bit width compared to previous vs default (34 bits etc)

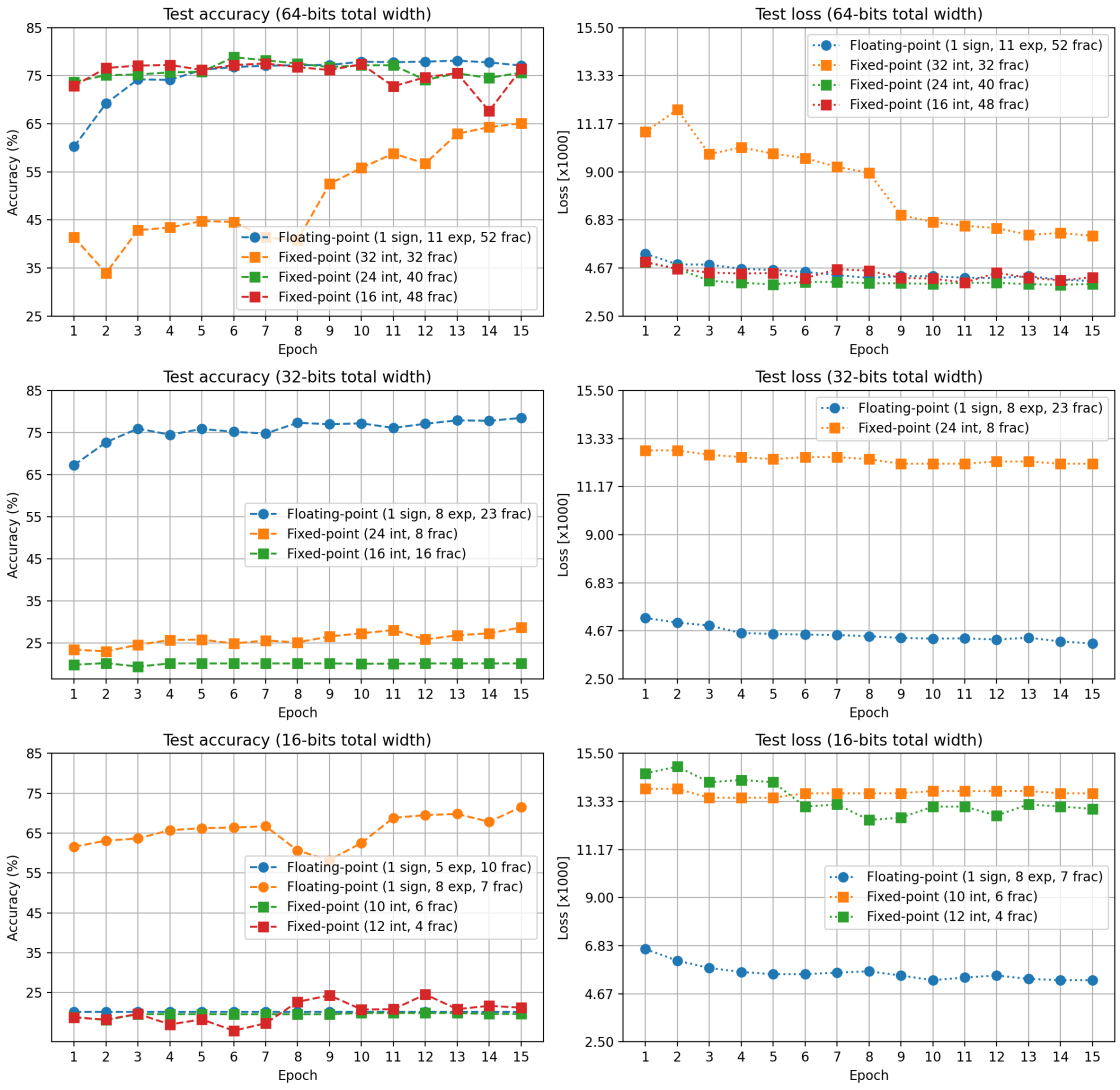

Figure 5.7: Performance against epochs for floating-point and fixed-point models.

say how we dont do synthesis due to time limitations, and its mostly no problem as the widhts are linear with hardware resources aside from the situations in which a dsp can be avoided (34 vs 35 bits etc)

Maybe talk about how correlation was verified

starting with integer or fractional in the search didnt seem to matter in the limited tests

Discuss the used parameters (ratio of positive and negative tolerance etc.) and how they affect the results

|

|

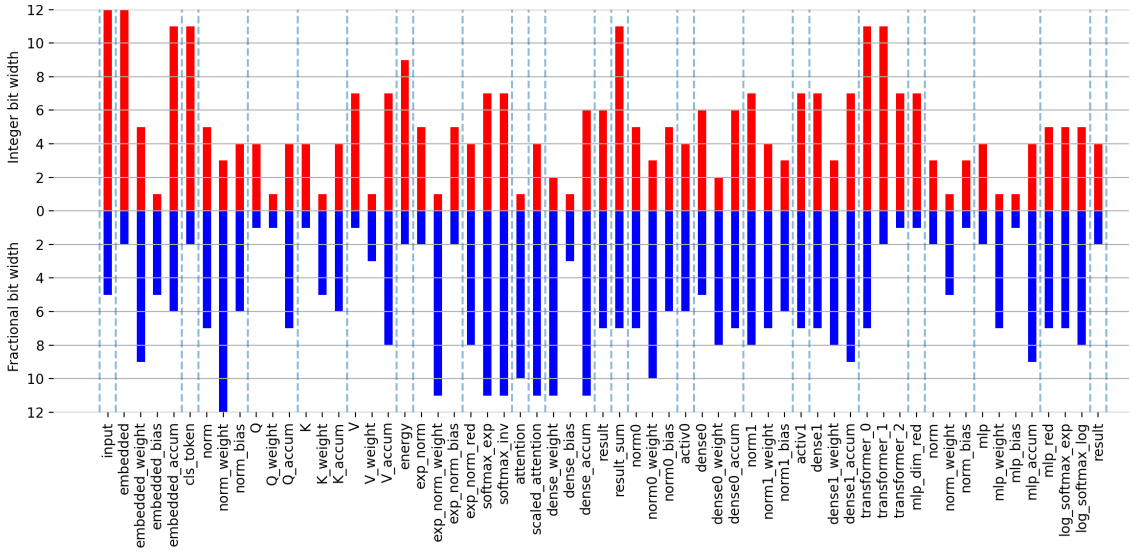

Figure 5.8: Visualization of the fixed-point precision of the types used in the accuracy-focused model.

Chapter 6

Conclusion

Conclude after writing all other sections, recapping the motivation, proposed model use cases, meta-programming approaches, how it all ties together and extends hardware-software co-design

|

|

|

6.1 Achievements

|

|

|

|

6.2 Discussion

|

|

|

|

6.3 Future Work

Bullet points or subsections

e.g. fuse batch norm to linear, pruning

Newer, efficient transformers like e.g. sparse transformer, low-rank transformer

this work didnt touch energy consumption

post-training novel method could use a faster simulation and some synthesis resource model to allow for a more sophisticated algorithm

|

|

References

[1] CERN. Jets at CMS and the determination of their energy scale | CMS experiment, .

[2] Josh Cogan, Michael Kagan, Emanuel Strauss, and Ariel Schwartzman. Jet-images: computer vision inspired techniques for jet tagging. *The journal of high energy physics*, 2015(2):1–16, Feb 18, 2015. doi: 10.1007/JHEP02(2015)118. URL https://link.springer.com/article/10.1007/JHEP02(2015)118.

[3] Luke de Oliveira, Michael Kagan, Lester Mackey, Benjamin Nachman, et al. Jet-images - deep learning edition. *The journal of high energy physics*, 2016(7):1–32, Jul 13, 2016. doi: 10.1007/JHEP07(2016)069. URL https://link.springer.com/article/10.1007/JHEP07(2016)069.

[4] Liam Moore, Karl Nordstrom, Sreedevi Varma, and Malcolm Fairbairn. Reports of my demise are greatly exaggerated: n-subjettiness taggers take on jet images. *SciPost physics*, 7(3):036, Sep 24, 2019. doi: 10.21468/SciPostPhys.7.3.036. URL https://hal.archives-ouvertes.fr/hal-01851157.

[5] Farah Fahim, Benjamin Hawks, Christian Herwig, James Hirschauer, et al. hls4ml: An open-source codesign workflow to empower scientific low-power machine learning devices. Mar 9, 2021. URL https://arxiv.org/abs/2103.05579.

[6] Harvey B. Newman, Avikar Periwal, Maria Spiropulu, Javier M. Duarte, et al. JEDI-net: a jet identification algorithm based on interaction networks. *The European physical journal. C, Particles and fields*, 80(1):1–15, Aug 14, 2019. doi: 10.1140/epjc/s10052-020-7608-4. URL http://cds.cern.ch/record/2688535.

[7] Abdelrahman Elabd, Vesal Razavimaleki, Shi-Yu Huang, Javier Duarte, et al. Graph neural networks for charged particle tracking on FPGAs. Dec 3, 2021. URL https://arxiv.org/abs/2112.02048.

[8] Xinyang Yuan. Constituentnet: Learn to solve jet tagging through attention. Technical report, -09-22 2021.

[9] K. Krasnov and R. Percacci. Gravity and unification: a review. *Classical and quantum gravity*, 35(14):143001, Jun 14, 2018. doi: 10.1088/1361-6382/aac58d. URL https://iopscience.iop.org/article/10.1088/1361-6382/aac58d.

[10] J. Walz, P. Grandemange, B. Vallage, et al. The GBAR antimatter gravity experiment. Technical Report 233, Springer International Publishing, 2015. URL http://cds.cern.ch/record/2055685.

[11] D. Pagano, M. Caccia, J. Fesel, S. Gerber, et al. Gravity and antimatter: the AEgIS experiment at CERN. Technical Report 1342, IOP Publishing, 2020. URL http://cds.cern.ch/record/2714100.

[12] Brian Greeene. How the higgs boson was found, July 2013. URL https://www.smithsonianmag.com/science-nature/how-the-higgs-boson-was-found-4723520/.

[13] Trigger, DAQ and FPGAs. URL http://www.hep.ph.imperial.ac.uk/~tapper/lecture/trigger.pdf.

[14] Sean Keane. CERN's large hadron collider restarts after three-year upgrade. URL https://www.cnet.com/science/cerns-large-hadron-collider-restarts-after-three-year-upgrade/.

[15] Alex Tapper. Triggering at collider experiments. URL http://www.hep.ph.imperial.ac.uk/~tapper/lecture/CMSIndia-2020.pdf.

[16] E. Coleman, M. Freytsis, A. Hinzmann, M. Narain, et al. The importance of calorimetry for highly-boosted jet substructure. *Journal of instrumentation*, 13(1):T01003, Jan 9, 2018. doi: 10.1088/1748-0221/13/01/T01003. URL https://search.proquest.com/docview/2365693051.

[17] Maurizio Pierini, Javier Mauricio Duarte, Nhan Tran, and Marat Freytsis. HLS4ML LHC jet dataset (30 particles), . URL https://doi.org/10.5281/zenodo.3601436.

[18] Maurizio Pierini, Javier Mauricio Duarte, Nhan Tran, and Marat Freytsis. HLS4ML LHC jet dataset (50 particles), . URL https://doi.org/10.5281/zenodo.3601443.

[19] Maurizio Pierini, Javier Mauricio Duarte, Nhan Tran, and Marat Freytsis. HLS4ML LHC jet dataset (100 particles), . URL https://doi.org/10.5281/zenodo.3602254.

[20] Maurizio Pierini, Javier Mauricio Duarte, Nhan Tran, and Marat Freytsis. HLS4ML LHC jet dataset (150 particles), . URL https://doi.org/10.5281/zenodo.3602260.

[21] Matteo Cacciari, Gavin P. Salam, and Gregory Soyez. The anti-kt jet clustering algorithm. *The journal of high energy physics*, 2008:063, Apr 1, 2008. doi: 10.1088/1126-6708/2008/04/063. URL http://iopscience.iop.org/1126-6708/2008/04/063.

[22] Edward Kreinar, Jennifer Ngadiuba, Zhenbin Wu, Philip Harris, et al. Fast inference of deep neural networks in FPGAs for particle physics. Technical Report 13, Institute of Physics (IOP), Apr 16, 2018. URL http://cds.cern.ch/record/2316331.

[23] Edward Kreinar, Jennifer Ngadiuba, Zhenbin Wu, Philip Harris, et al. Fast inference of deep neural networks in FPGAs for particle physics. Technical Report 13, IOP Publishing, Apr 16, 2018. URL http://cds.cern.ch/record/2316331.

[24] G. Valentino, R. W. Assmann, R. Bruce, and N. Sammut. Classification of LHC beam loss spikes using support vector machines. pages 355–358. IEEE, Jan 2012. doi: 10.1109/SAMI.2012.6208988. URL https://ieeexplore.ieee.org/document/6208988.

[25] Tianqi Chen and Tong He. Higgs Boson Discovery with Boosted Trees. In Glen Cowan, Cecile Germain, Isabelle Guyon, Balázs Kegl, and David Rousseau, editors, *Proceedings of the NIPS 2014 Workshop on High-energy Physics and Machine Learning*, volume 42 of *Proceedings of Machine Learning Research*, pages 69–80, Montreal, Canada, 13 Dec 2015. PMLR. URL https://proceedings.mlr.press/v42/chen14.html.

[26] Andrzej Skoczen, Maciej Wielgosz, and Matej Mertik. Using LSTM recurrent neural networks for monitoring the LHC superconducting magnets. Technical Report 867, Elsevier B.V, Nov 18, 2016. URL http://cds.cern.ch/record/2234465.

[27] Jie Ren, Lei Wu, and Jin Min Yang. Unveiling CP property of top-higgs coupling with graph neural networks at the LHC. *Physics letters. B*, 802:135198, Mar 10, 2020. doi: 10.1016/j.physletb.2020.135198. URL https://dx.doi.org/10.1016/j.physletb.2020.135198.

[28] Edward Kreinar, Zhenbin Wu, Gianluca Cerminara, Kinga Wozniak, et al. Distance-weighted graph neural networks on FPGAs for real-time particle reconstruction in high energy physics. Technical Report 3, Frontiers Media S.A, 2020. URL http://cds.cern.ch/record/2728798.

[29] Abdelrahman Elabd, Vesal Razavimaleki, Shi-Yu Huang, Javier Duarte, et al. Graph neural networks for charged particle tracking on FPGAs. Dec 3, 2021. URL https://arxiv.org/abs/2112.02048.

[30] Gil Keren and Bjorn Schuller. Convolutional RNN: An enhanced model for extracting features from sequential data. pages 3412–3419. IEEE, Jul 2016. doi: 10.1109/IJCNN.2016.7727636. URL https://ieeexplore.ieee.org/document/7727636.

[31] Jan Chorowski, Dzmitry Bahdanau, Dmitriy Serdyuk, Kyunghyun Cho, et al. Attention-based models for speech recognition. Jun 24, 2015. URL https://arxiv.org/abs/1506.07503.

[32] Ashish Vaswani, Noam Shazeer, Niki Parmar, Jakob Uszkoreit, et al. Attention is all you need. Jun 12, 2017. URL https://arxiv.org/abs/1706.03762.

[33] Ashish Vaswani, Samy Bengio, Eugene Brevdo, Francois Chollet, Aidan N. Gomez, Stephan Gouws, Llion Jones, Łukasz Kaiser, Nal Kalchbrenner, Niki Parmar, Ryan Sepassi, Noam Shazeer, and Jakob Uszkoreit. Tensor2tensor for neural machine translation. *CoRR*, abs/1803.07416, 2018. URL http://arxiv.org/abs/1803.07416.

[34] Jay Alammar. The illustrated transformer. URL https://jalammar.github.io/illustrated-transformer/.

[35] Mohammadreza Najafi, Kaiwen Zhang, Mohammad Sadoghi, and Hans-Arno Jacobsen. Hardware acceleration landscape for distributed real-time analytics: Virtues and limitations. pages 1938–1948. IEEE, Jun 2017. ISBN 1063-6927. doi: 10.1109/ICDCS.2017.194. URL https://ieeexplore.ieee.org/document/7980135.

[36] Dagli and Lammers. Possible applications of neural networks in manufacturing. page 605 vol.2. IEEE TAB Neural Network Committee, 1989. doi: 10.1109/IJCNN.1989.118423. URL https://ieeexplore.ieee.org/document/118423.

[37] Cathy Wu, Michael Berry, Sailaja Shivakumar, and Jerry McLarty. Neural networks for full-scale protein sequence classification: Sequence encoding with singular value decomposition. *Machine learning*, 21(1):177, Oct 1, 1995. doi: 10.1023/A:1022677900508.

[38] Vincent Vanhoucke, Andrew Senior, and Mark Z. Mao. Improving the speed of neural networks on CPUs. In *Deep Learning and Unsupervised Feature Learning Workshop, NIPS 2011*, 2011.

[39] Sainathan Ganesh Iyer and Anurag Dipakumar Pawar. GPU and CPU accelerated mining of cryptocurrencies and their financial analysis. pages 599–604. IEEE, Aug 2018. doi: 10.1109/I-SMAC.2018.8653733. URL https://ieeexplore.ieee.org/document/8653733.

[40] Gang Chen, Haitao Meng, Yucheng Liang, and Kai Huang. GPU-accelerated real-time stereo estimation with binary neural network. *IEEE transactions on parallel and distributed systems*, 31(12):2896–2907, Dec 1, 2020. doi: 10.1109/TPDS.2020.3006238. URL https://ieeexplore.ieee.org/document/9130887.

[41] Qianru Zhang, Meng Zhang, Tinghuan Chen, Zhifei Sun, et al. Recent advances in convolutional neural network acceleration. *Neurocomputing (Amsterdam)*, 323:37–51, Jan 5, 2019. doi: 10.1016/j.neucom.2018.09.038. URL https://dx.doi.org/10.1016/j.neucom.2018.09.038.

[42] Graphcore. Graphcore intelligence processing unit. URL https://www.graphcore.ai/products/ipu.

[43] Phil Knag, Jung Kuk Kim, Thomas Chen, and Zhengya Zhang. A sparse coding neural network ASIC with on-chip learning for feature extraction and encoding. *IEEE journal of solid-state circuits*, 50(4):1070–1079, Apr 2015. doi: 10.1109/JSSC.2014.2386892. URL https://ieeexplore.ieee.org/document/7015626.

[44] K. Venkata Ramanaiah and Cyril Prasanna Raj. ASIC implementation of neural network based image compression. *International Journal of Computer Theory and Engineering*, pages 494–498, 2011. doi: 10.7763/IJCTE.2011.V3.356.

[45] Andrew Boutros, Sadegh Yazdanshenas, and Vaughn Betz. You cannot improve what you do not measure. *ACM transactions on reconfigurable technology and systems*, 11(3):1–23, Dec 22, 2018. doi: 10.1145/3242898. URL http://dl.acm.org/citation.cfm?id=3242898.

[46] Eriko Nurvitadhi, Ganesh Venkatesh, Jaewoong Sim, Debbie Marr, et al. Can FPGAs beat GPUs in accelerating next-generation deep neural networks? FPGA '17, pages 5–14. ACM, Feb 22, 2017. doi: 10.1145/3020078.3021740. URL http://dl.acm.org/citation.cfm?id=3021740.

[47] Yixing Li, Zichuan Liu, Kai Xu, Hao Yu, et al. A GPU-outperforming FPGA accelerator architecture for binary convolutional neural networks. *ACM journal on emerging technologies in computing systems*, 14(2):1–16, Jul 27, 2018. doi: 10.1145/3154839. URL http://dl.acm.org/citation.cfm?id=3154839.

[48] Eriko Nurvitadhi, David Sheffield, Jaewoong Sim, Asit Mishra, et al. Accelerating binarized neural networks: Comparison of FPGA, CPU, GPU, and ASIC. pages 77–84. IEEE, Dec 2016. doi: 10.1109/FPT.2016.7929192. URL https://ieeexplore.ieee.org/document/7929192.

[49] Eriko Nurvitadhi, Jaewoong Sim, David Sheffield, Asit Mishra, et al. Accelerating recurrent neural networks in analytics servers: Comparison of FPGA, CPU, GPU, and ASIC. pages 1–4. EPFL, Aug 2016. doi: 10.1109/FPL.2016.7577314. URL https://ieeexplore.ieee.org/document/7577314.

[50] Sakari Lahti, Panu Sjovall, Jarno Vanne, and Timo D. Hamalainen. Are we there yet? a study on the state of high-level synthesis. *IEEE transactions on computer-aided design of integrated circuits and systems*, 38(5):898–911, May 2019. doi: 10.1109/TCAD.2018.2834439. URL https://ieeexplore.ieee.org/document/8356004.

[51] CERN. Facts and figures about the LHC | CERN, . URL https://home.cern/resources/faqs/facts-and-figures-about-lhc.

[52] R. Guida, M. Capeans, and B. Mandelli. Characterization of RPC operation with new environmental friendly mixtures for LHC application and beyond. *Journal of Instrumentation*, 11(07):C07016–C07016, jul 2016. doi: 10.1088/1748-0221/11/07/c07016. URL https://doi.org/10.1088/1748-0221/11/07/c07016.

[53] M. Capeans, R. Guida, and B. Mandelli. Strategies for reducing the environmental impact of gaseous detector operation at the CERN LHC experiments. *Nuclear Instruments and Methods in Physics Research Section A: Accelerators, Spectrometers, Detectors and Associated Equipment*, 845:253–256, 2017. doi: https://doi.org/10.1016/j.nima.2016.04.067. URL https://www.sciencedirect.com/science/article/pii/S0168900216302807. ID: 271580.

[54] Kaiming He, Xiangyu Zhang, Shaoqing Ren, and Jian Sun. Deep residual learning for image recognition. pages 770–778. IEEE, Jun 2016. doi: 10.1109/CVPR.2016.90. URL https://ieeexplore.ieee.org/document/7780459.

[55] Christian Szegedy, Sergey Ioffe, Vincent Vanhoucke, and Alex Alemi. Inception-v4, inception-resnet and the impact of residual connections on learning. Feb 23, 2016. URL https://arxiv.org/abs/1602.07261.

[56] Hongxiang Fan, Shuanglong Liu, Martin Ferianc, Ho-Cheung Ng, et al. A real-time object detection accelerator with compressed SSDLite on FPGA. pages 14–21. IEEE, Dec 2018. doi: 10.1109/FPT.2018.00014. URL https://ieeexplore.ieee.org/document/8742299.

[57] Patrick Shaumont. Fixed point arithmetic in DSP — real time digital signal processing. URL https://schaumont.dyn.wpi.edu/ece4703b21/lecture6.html.

[58] Raghuraman Krishnamoorthi, Seth Weidman, and Jerry Zhang. Static quantization with eager mode in pytorch. URL https://pytorch.org/tutorials/advanced/static_quantization_tutorial.html.

[59] Abhishek Sharma. Pytorch JIT and torchscript. URL https://towardsdatascience.com/pytorch-jit-and-torchscript-c2a77bac0fff.

[60] Jerry Zhang. FX graph mode quantization user guide. URL https://pytorch.org/tutorials/prototype/fx_graph_mode_quant_guide.html.

[61] Alessandro Pappalardo. Xilinx/brevitas, 2021. URL https://doi.org/10.5281/zenodo.3333552.

[62] Tianyi Zhang, Zhiqiu Lin, Guandao Yang, et al. QPytorch: A low-precision arithmetic simulation framework, 2019.

[63] Alan H. Barr. The einstein summation notation. *An Introduction to Physically Based Modeling (Course Notes 19), pages E*, 1:57, 1991.

[64] Pierre Blanchard, Desmond J. Higham, and Nicholas J. Higham. Accurate computation of the log-sum-exp and softmax functions. *arXiv preprint arXiv:1909.03469*, 2019.

[65] Kuan Wang, Zhijian Liu, Yujun Lin, Ji Lin, et al. HAQ: Hardware-aware automated quantization with mixed precision. pages 8604–8612. IEEE, Jun 2019. doi: 10.1109/CVPR.2019.00881. URL https://ieeexplore.ieee.org/document/8954415.

Appendices

Appendix A

Something

something

Notes